2. TOPICS ON RANKINE CYCLE POWER SYSTEMS TECHNOLOGY

Martin J. Saari, Jack A. Heller, Robert G. Dorsch, Phillip L. Stone, Herbert G. Hurrell, Martin V. Gutstein, and Cavour H. Hauser

The preceding discussion on nuclear reactors dealt with some of the technical aspects of the thermal energy source and transport of this energy to the power conversion system. The purpose of the following discussion is to review selected topics associated with that part of the Rankine power system that converts the thermal energy into the mechanical energy used to drive the electric generating equipment. The substance of this discussion has been accumulated through research and development programs conducted at the Lewis Research Center and under NASA contracts and grants to industry and universities. All this effort has been targeted at the development of power systems for space flight applications.

The space Rankine system (fig. 2-1) has a fundamental similarity to the ground-based power system (fig. 2-2) but differs substantially in size, weight, and power output. The basic difference in cycle operating conditions results from the fact that in the space environment waste heat from the system must be dissipated by radiation rather than by convection as in the ground-based system. Thus, since the size (and weight) of the radiator is a function of the fourth power of the radiating temperature, there is a strong incentive to operate the heat rejection radiator at as high a temperature as possible. To maximize cycle efficiency it is necessary to elevate the peak cycle temperatures (at the turbine inlet) to the highest levels commensurate with material limitations. Typically, then, the Rankine space-power systems operate at turbine inlet temperatures between 1200° and 2000° F, depending on the working fluids used. In contrast, the ground-based steam-power systems characteristically operate at temperatures below 1200° F.

Because of the high temperatures, the space-power systems utilize liquid metals as working fluids to minimize the peak pressure levels which reflect in reduced system weight. The peak cycle pressure levels thus range between 50 and 300 psia for the working fluids currently under consideration. The peak pressures in the steam systems, on the other hand, range between 1000 to 5000 psia.

Despite the differences in temperatures, pressures, working fluids, and physical size between the space-power system and ground-based powerplant, the basic

thermodynamic and hydrodynamic processes that occur within either system are, nonetheless, governed by the same physical principles which provide the path for cross fertilization of technological advances in either direction. In fact, many of the liquid metal heat-transfer and fluid dynamic problems have been investigated experimentally by using water or organic fluids because of the similarity of behavior characteristics and the relative ease of handling these fluids.

The pressing necessity for minimum weight and size of space-power systems has stimulated an extensive search, during the past decade, for ways and means of maximizing performance from each pound and each cubic inch of hardware without losing sight of the crucial reliability and long-life requirement. The Rankine system technology has, for the most part, been acquired through the Systems for Nuclear Auxiliary Power Development (SNAP) programs and more recently through research activities directed toward the development of advanced nuclear Rankine space-power systems.

The discussion is presented, not on the pretense of having a pat answer to any specific related problem, but hopefully for the purpose of stimulating further thought and inquiry into potential application of ideas to either the conventional fossil-fuel or reactor-powered ground-based electric generating systems. The subjects to be considered include the following:

(1) Thermal design considerations and stability of compact once-through boilers
(2) Turbine-blade erosion
(3) Some cogent materials considerations
(4) Pump technology
(5) Analysis of system dynamics by computer simulation

TECHNOLOGY OF COMPACT "ONCE-THROUGH" BOILERS

In a "once-through" boiler, the boiling fluid enters as a liquid, discharges as a saturated or superheated vapor, and flows directly to the turbine without the need for liquid-vapor separation or liquid recirculation. In space boilers, the heating fluid enters the boiler, as shown in figure 2-3, in the region of the vapor outlet. The heating fluid then flows opposite to or countercurrent to the flow of the boiling fluid and discharges in the region of the boiling fluid inlet. A typical temperature profile in such a boiler is also shown in figure 2-3. The temperatures of both the heating and the boiling fluids are plotted as a function of distance along the boiler. The heating fluid, in passing through the heat exchanger, transfers heat to the boiling fluid. Consequently, its temperature decreases continuously. The boiling fluid, entering opposite to the heating fluid, is quickly heated to its boiling temper-

ature corresponding to the local pressure. Thereafter, in the boiling region, the temperature decreases somewhat. This temperature decrease is due to the pressure loss incurred by the boiling fluid and to the fact that the temperature is related to the pressure in a two-phase fluid. At the end of the boiling region, further additions of heat cause the temperature of the boiling fluid to increase. This region is called the superheated vapor region.

The temperature difference between the heating and boiling fluids at the boiler inlet is generally very large, of the order of several hundred degrees. This temperature difference decreases rapidly, however, and reaches a minimum at the point where boiling first initiates. This minimum temperature difference between the heating and boiling fluids is called the "pinch-point" temperature difference. In the boiling region, the temperature difference increases again. In the superheated vapor region, the temperature difference decreases.

As the boiling fluid undergoes a transformation from a liquid to a vapor, its character changes radically. This can be explained by reference to figure 2-4, which shows a schematic of a simple once-through hollow-tube boiler. The heating fluid flows in the annulus, and the boiling fluid flows in the central tube opposite in direction to the heating fluid. As the boiling fluid is heated, bubbles are produced at the tube wall and these are swept into the center of the tube. This flow regime is called the "bubbly" flow regime. Further downstream, the bubbles agglomerate into single large bubbles which almost fill the entire cross section of the tube. This regime is called the "plug" or "slug" flow regime. With further heat addition, the plugs tend to enlarge and burst open, leaving a ring or annulus of liquid at the tube wall and droplets traveling with the vapor in the core. This regime is frequently labeled the "annular" or "annular-mist" flow regime. Eventually, the liquid layer at the wall is boiled or evaporated, and a "dry-wall" condition exists along with droplets flowing in the vapor core. This flow regime is called the "mist" or "fog" flow regime. Figure 2-4 also shows schematically the heat flux distribution along the length of the single-tube boiler. At the inlet, the heat flux in the liquid convective region is moderately high but decreases with length. This decrease is due to the reduction of temperature difference between the heating and boiling fluids. In the boiling region, the heat flux increases to a maximum. The maximum flux generally occurs at the end of the annular flow regime. Thereafter, the flux decreases substantially to values typical of vapor convection. This is not unexpected since a continuous liquid layer at the tube wall does not exist in this region of the boiler. The heat flux decreases with length due again to the decrease in temperature difference between the heating and boiling fluids. Because of the poor heat-transfer characteristics at this location, extraordinarily long tube lengths would be required to evaporate most of the entrained liquid droplets flowing in the vapor.

Space boilers are made more compact not only by bringing the parts of a boiler closer together, such as by reducing the separation between tubes, but also by increasing the average heat flux. Higher average heat fluxes are achieved by separating the liquid and vapor phases within the tubes by swirling the flow as shown in figure 2-5. When a swirl is induced in the flow, the liquid droplets are centrifuged to the tube wall where efficient boiling heat transfer can take place. Moreover, when the liquid is separated out, the vapor then has a relatively large, unobstructed passage for it to flow to the outlet of the boiler. The effect on the heat flux distribution is also shown in figure 2-5. The heat fluxes in the liquid and low-quality regions for the two cases are comparable. The biggest difference occurs in the boiling region. The swirl effect on the liquid droplets causes the boiling region to extend to higher qualities, and thereby the average heat flux is increased substantially. In the vapor region, the swirl effect increases the effective velocity which raises the local heat-transfer coefficients and hence the heat flux. This increase in the heat flux can be significant depending on the requirements for dryness and superheat.

To swirl the flow, inserts such as those illustrated in figure 2-6 are placed inside the tubes of a boiler. The twisted tape, fabricated from a flat strip of sheet metal and then twisted, is thus one of the simplest inserts. However, the tape divides the tube into two distinct flow passages. If the insert is fabricated or installed improperly, the hydraulic resistance of the two passages can differ substantially, and this may lead to maldistributions of flow and heat transfer. To avoid this potential problem, the helical vane on a center rod has been employed in boiler tubes. This insert has the advantage that the vane extends along a tube radius and not a diameter. Consequently, it swirls the boiling fluid without dividing the tube into two flow passages. Both the twisted tape and the helical vane have surfaces along the tube axis where the centrifugal forces are small or nonexistent. As a result, some of the liquid in the boiling fluid can flow along these surfaces and thus bypass the tube wall. If the insert extends to the outlet end of the boiler, it is possible that some of this liquid could flow the entire length of the boiler and exit with the vapor. Frequently these inserts are terminated upstream of the boiler exit. The liquid will then flow off the insert, be centrifuged to the tube wall, and then be evaporated before exiting the boiler.

The helical wire coil insert has been employed in boilers because of its ease of manufacture and installation. The coil is placed inside a tube in an extended condition and then allowed to relax, expand radially, and thus engage the tube wall. In addition, liquid bypassing of the tube wall is minimized since this insert has no surfaces near the tube centerline. The combination of a wire coil and a center rod is employed in the liquid and low-quality regions of a boiler to increase the fluid

velocities and hence the heat-transfer coefficients.

A comparison of the performance of a given boiler tube both with and without a swirl-generating insert is shown schematically in figure 2-7. The curves shown in this figure represent a composite of experimental data obtained with conventional fluids, such as boiling water and organic fluids, and with liquid metals, such as boiling potassium. Local heat-transfer coefficients are plotted as a function of length along the tube. Generally, the tube with an insert has higher heat-transfer coefficients and a longer boiling region than the tube without an insert. Moreover, at the outlet, the tube without a swirl insert discharges an intermediate quality mixture of liquid and vapor. For example, conventional fluids discharge from a short hollow-tube boiler with a maximum exit quality of about 60 percent. High conductivity fluids, such as potassium, discharge at an exit quality as high as 90 percent. However, the same tube with an insert discharges a superheated vapor, superheated by as much as 200° F. The length of the hollow-tube boiler would have to be substantially greater than that of the boiler with an insert to discharge a vapor with the same superheat. For a given length, the tube with an insert has a much larger pressure drop than the tube without an insert. However, the hollow tube, to achieve an exit superheat of 200° F, for example, would be much longer than the tube with an insert. Its pressure drop, therefore, may not be much different from the tube with an insert. In general, the pressure drop penalty associated with the use of inserts must be evaluated for each individual boiler.

The reduction in length of space boilers made possible through the use of swirl-generating inserts is shown in figure 2-8. The length of the boiler with hollow tubes has been taken as unity. The boiler that contains inserts in its tubes is shown to have a length one-fourth or less that of the hollow-tube boiler. The specific volumes (i.e., the volume of a boiler per kilowatt of heat transferred) or three typical boilers: a fossil-fueled central power station boiler, a sodium-steam boiler of a nuclear central power system, and a liquid metal-to-liquid metal space-power boiler are compared in figure 2-9. The specific volume of the sodium-steam boiler is roughly one-tenth that of the fossil-fueled boiler. This is primarily attributable to the superior heat-transfer characteristics of liquid metals as compared to the combustion gases. Space boilers also employ liquid metals, but their specific volumes are still smaller than the sodium-steam generator, as shown in the figure. Part of this reduction of specific volume is due to the lower working pressures of the liquid metal boiling fluid (well below critical pressure) which permits the use of thin-wall tubing. (The thin-wall tubing offers lower resistance to the transfer of thermal energy.) A substantial portion of this reduction in volume of space boilers, however, is due to the application of swirl-flow technology and the use of inserts, as described previously. It is possible that ground-based boilers may be made

more compact through the use of this same technology. However, the magnitude of the reduction in boiler size depends on the characteristics of each boiler and, thus, must be individually determined.

Figure 2-10 shows a boiler now being tested for the SNAP-8 space-power system. The boiler is a once-through counterflow heat exchanger. The heating fluid is a sodium-potassium alloy (NaK), and the boiling fluid is mercury. The mercury flows in seven tubes contained within the shell. Each tube possesses a swirl-generating insert. Approximately 500 kilowatts of heat are transferred at a mercury vapor exit temperature of nearly 1300° F. The coiled configuration of the boiler reduces thermal stresses and facilitates installation of the boiler on the spacecraft. The diameter of the coil is 48 inches, and the height is approximately 36 inches.

The SNAP-8 boiler has a feature which may be of interest for the design of the sodium-steam generator of the ground-based reactor powerplant. The tubes of this boiler are designed with double containment - that is, with two walls separating the boiling fluid from the heating fluid. In the sodium-steam generator, such a design would reduce the likelihood of mixing water with sodium. In the SNAP-8 system, double containment minimizes the possibility of mixing the mercury with the heating fluid which is the reactor coolant.

The double containment feature is shown in figure 2-11. This figure shows a cross section of the SNAP-8 boiler. The outer pipe is the shell which contains the flowing NaK heating fluid. Inside the shell are the seven double-walled tubes. Mercury boils inside the inner wall and nonflowing NaK fills the space between the walls. A leak between the flowing NaK and the static NaK would not affect the operation of the boiler. A leak between the mercury and the static NaK would allow the higher pressure mercury to flow into the static NaK but not into the NaK that passes through the reactor. Although the double containment concept is somewhat complicated, it does provide greater reliability and safety than single containment.

BOILER INSTABILITIES

High-flux short-tube boilers are known to exhibit a wide variety of flow, pressure, and steam void fluctuations and oscillations. These disturbances are generally referred to as boiler instabilities. However, these instabilities are caused by a variety of different mechanisms, depending on the boiler and system operating conditions and on the particular hardware characteristics. It is necessary, therefore, to identify the specific type of instability which is occurring before an attempt can be made to reduce or eliminate it.

Three frequently encountered types of boiler instabilities, which will be used as examples, are the following:

(1) Acoustic

(2) Heat-transfer coupled

(3) Feed-system coupled

  (a) Excursions

  (b) Dynamic oscillations

The acoustic type is an example of a channel flow disturbance; the heat-transfer coupled is typical of an instability which is internally coupled within the boiler; and the feed-system coupled is an example of a system-coupled instability.

Acoustic disturbances in boiler tubes or heated channels are related to the fact that a very low speed of sound exists in a boiling fluid. The propagation velocity of a pressure wave through the very low-quality subcooled boiling region is shown in figure 2-12 as a function of the amount of steam present in the form of bubbles in the liquid. The curve is based on data taken by Karplus at Armour Research Foundation under government sponsorship. With no steam bubbles present, the wave velocity through the liquid is about 4800 feet per second. This velocity decreases sharply to 300 feet per second with only $1\frac{1}{2}$ percent steam in the tube. This happens because the presence of even a small amount of vapor causes a very large increase in compressibility of the fluid. At 40 percent steam, the velocity is down to only 60 feet per second.

The low speed of sound in the subcooled boiling region makes it possible for "organ-pipe" type pressure wave resonances to occur in very short tube lengths. For a 30 cps resonance, for example, these lengths are of the order of 1 to 5 feet as compared to 80 feet for a liquid-filled tube. These resonant pressure waves can be self-sustaining under some conditions.

The low acoustic speed in a boiling fluid also permits another type of disturbance to occur in the higher quality net vaporization region, that is, between 50 and 100 percent steam by volume. In this region the sonic velocity and the fluid velocity in the tube can be comparable in magnitude particularly at high weight flow rates. Thus, choked flow conditions can occur. In fact, it is possible for the fluid velocity to actually be higher than the acoustic velocity and have local supersonic flow accompanied by shock waves. Thus, in an unsteady flow situation, there is a mechanism for intermittent choking and/or shock wave formation. The resultant pressure wave disturbances may also cause water hammer effects through the evaporation of droplets and the collapse of vapor bubbles as they travel through the boiler tube.

Acoustic disturbances are encountered mostly in startup or transient situations and usually do not cause serious operating-point instabilities. This is because the

disturbances occur mostly at high frequencies (between 20 and 400 cps) or are random with time. In either case, they cannot couple with the other system components. When these acoustic disturbances do occur, they may cause problems in the boiler such as inducing mechanical vibration of the boiler tubes. Adjustments in either the tube flow rate, the subcooling, or the heating rate may sometimes be necessary to reduce or eliminate an acoustic disturbance.

The second example is the heat-transfer-coupled instability. This instability has been experienced during developmental testing of the SNAP-8 boiler. It is an oscillatory type of instability; that is, it manifests itself as periodic oscillations in boiler exit pressure. This instability results from a coupling process internal to the boiler because it has been observed when all the boiler input variables, such as liquid flow, were constant. It seems to be caused by an interaction between the heat flux within the boiler and the vapor generation rate. This is believed because the pressure oscillations correlate quite well with the pinch-point temperature difference, which is a measure of heat flux.

As noted earlier (in the discussion of fig. 2-3), at the end of the subcooled region where boiling starts, the fluids are separated by a rather small temperature difference, or pinch-point ΔT. Experimental correlations between the exit pressure oscillations and the pinch-point ΔT are shown in figure 2-13. The amplitude of the boiler exit pressure oscillation is plotted against the pinch-point ΔT for three different flow rates of the boiling mercury. At large values of the pinch-point ΔT, the amplitude was only 1 or 2 percent of the mean pressure. However, the amplitude was found to increase sharply as the pinch-point ΔT was decreased for a given mercury flow rate.

The frequency of this pressure oscillation was in the range of 0.1 to 1 cps. As the figure suggests, the effect of this instability can be kept at a tolerable level by operating the boiler with a high value of pinch-point ΔT.

It should be mentioned that the pinch-point temperature difference ΔT should not be increased indiscriminately, because an excessively large temperature difference has an adverse effect on heat transfer. The upper and lower limits on pinch-point ΔT are influenced by the working fluids and boiler tube geometry.

The third example is the feed-system-coupled instability, which involves an interaction between boiler pressure and the liquid flow into the boiler tubes. In the excursive type of feed-system-coupled instability, a flow excursion can occur because of the peculiar relation which exists between boiler pressure and weight flow rate at some operating conditions. A typical plot of steady-state boiler tube inlet pressure against weight flow rate for a hollow-tube boiler is shown in figure 2-14. The curve is for constant heat input, and for simplicity, the exit pressure is assumed to remain constant. The inlet pressure is, of course, equal to the exit

pressure plus the pressure drop in the tube at each flow rate. At low flow rates, the boiler tube exit quality is high and the tube contains mostly high velocity vapor. It is the high velocity vapor which accounts for most of the pressure drop in the tube. The pressure drop caused by the low velocity liquid is small. At low increasing flows, the inlet pressure, therefore, at first increases rapidly with an increasing weight flow. However, as the weight flow into the boiler tube continues to increase, the exit quality begins to decrease because less of the inlet flow is vaporized. This results in increasingly smaller fractions of high velocity vapor in the tube. At some point, therefore, the pressure starts to decrease and continues to do so until the flow becomes so large that there is only hot liquid in the tube. In the all-liquid region the pressure again increases with weight flow. The region in which the pressure decreases as the weight flow increases is called the negative-resistance region. It is bounded by positive-resistance regions on each side.

The implications of the positive- and negative-resistance regions on static stability are now examined. Portions of the boiler curve in these regions are replotted in figure 2-15 along with corresponding curves for the boiler feed water supply system.

First, the high-quality region with positive boiler resistance is examined (see fig. 2-14). A portion of this region is shown in detail on the left side of figure 2-15. The system is considered to be operating at the intersection point. The flow into the boiler is assumed to increase a small amount or ΔW. The boiler inlet pressure tends to become greater than the supply pressure and decelerate the flow. The increase in flow, therefore, cannot be maintained and the system returns to the operating point at the end of the transient. The system is thus statically stable.

Now the negative-resistance region of the boiler is examined (fig. 2-14). A portion of this region is shown in the center of figure 2-15. With the feed-system characteristics indicated, it is not possible to operate at the intersection point because a small flow increase ΔW would cause the boiler inlet pressure to begin to drop below the supply pressure. The flow would therefore accelerate and continue to increase. The system, which is thus unstable and would undergo a flow and pressure excursion, ends up in the stable positive-resistance region at high weight flows.

The third set of curves in figure 2-15 are now considered. The hydraulic characteristics of the feed system have been changed to give a steeper feed-system supply curve as indicated. The boiler and feed-system combination is not statically stable even though the boiler is operating in the negative-resistance region. The system is stable about the operating point because with a flow increase ΔW the supply pressure now cannot provide the higher pressure demanded by the boiler. The flow thus decelerates, and the system returns to the operating point. Conse-

quently, a boiler can be statically stabilized in the negative-resistance region by using a pump with a steeper slope or by adding a pressure drop orifice at the inlet to the boiler tube or by doing both.

From what has been discussed so far, feed-system-coupled instabilities would be expected when the boiler is operated in the negative-resistance region. In addition, it is often assumed that a once-through boiler having high-quality steam output and operating in the positive-resistance region will be stable. This assumption results from analyzing the system only from a steady-state viewpoint. However, in practice, feed-system-coupled boiler instabilities that are often encountered in the positive-resistance operating region are the dynamic type. They are oscillatory and occur at particular frequencies. The reason that dynamic oscillations can occur in the positive as well as in the negative-resistance region is that the pressure oscillation can lag behind the flow oscillation. It can lag to the point where the pressure is actually decreasing when the flow is increasing. That is, a negative-resistance condition can exist at a particular oscillation frequency. The lag is principally caused by the fact that it takes time for the liquid flow into the boiler to vaporize and thereby affect the boiler pressure.

In order to predict the occurrence of this type of instability the dynamic characteristics of the boiler must be known. Because relatively little is known in this area, fundamental research studies on the dynamic characteristics of simple heat exchanger boiler configurations are being conducted at the Lewis Research Center.

The boiler dynamics research rig is shown in figures 2-16 and 2-17. The boiler test section is a single-tube boiler heated by hot water. The liquid Freon pumped through the boiler tube is vaporized, and then it flows through a large diameter pipe to a large water-cooled condenser. This provides constant boiler exit pressure. Stable steady-state conditions are established in the boiler and then the Freon inlet flow is sinusoidally perturbed about its mean value by the controllable throttle valve. Boiler inlet perturbation pressures and flows are measured at the location shown in figure 2-16.

Forced-flow and pressure oscillations are measured at the boiler inlet and are shown schematically in figure 2-18. From data of this kind the amplitudes of the flow oscillation (A_F) and the pressure oscillation (A_P) are obtained at each imposed frequency. Further, at each frequency, the amount (in degrees) that the pressure oscillation lags behind the flow oscillation is determined.

Required at each frequency is the ratio of the sinusoidal pressure perturbation to the sinusoidal flow perturbation. This ratio, which is known as the boiler inlet impedance, is analogous to the ratio of voltage to current in an ac circuit.

It is convenient to plot this ratio in the polar form shown in figure 2-19. At a particular frequency the distance from the origin to the curve is the amplitude ratio

(A_P over A_F), and the angle measured from the positive axis is the pressure oscillation lag in degrees. When the amplitude ratio and lag angle are plotted for a series of different frequencies in the range of interest, a curve of the type shown is obtained. The curve starts at steady state (or zero frequency) with no lag between pressure and flow. This is therefore called the positive-resistance axis. The amplitude vector rotates clockwise with increasing frequency. At the point where the curve crosses the axis, the pressure oscillation lags behind the flow oscillation by 180^o; thus, the pressure is decreasing when the flow is increasing and vice versa. That is, the boiler has pure negative resistance at this frequency.

A similar plot of actual frequency response data taken on the boiler dynamics rig is shown in figure 2-20. A hollow single-tube boiler was operating stably at a point in the positive-resistance steady-state region, and forced oscillations were imposed at frequencies between 0.04 and 1.5 cps. The experimental results are shown by the solid curve. Shown as a broken curve are the analytical results calculated with the aid of a simple model. The shapes of these frequency response curves are dependent on the boiler tube geometry and on the particular operating conditions of the boiler. Therefore, all parameters used in the analytical calculations were evaluated at the operating point from the steady-state characteristics of the boiler tested.

The analytical model used is analogous to a short electric transmission line with a current time delay device located near the inlet end of the line. The agreement between the analytical results and experimental data is very good for a short hollow tube boiler of this type.

Both the experimental and the analytical curves indicate that the inlet impedance of the boiler has a negative-resistance component for frequencies between 0.2 and 1.2 cps. Further, at a frequency of about 0.5 cps the inlet impedance consists entirely of negative resistance. Thus, the boiler tested is a potential source of feed-system-coupled instabilities in this frequency range.

In order to determine whether an instability will actually occur, the impedance of the feed system at these frequencies must also be considered. The boiler inlet impedance curve from figure 2-20 is shown in figure 2-21 along with a corresponding polar plot of the feed-system impedance. Like the boiler, the feed-system impedance varies with frequency. However, it has a positive-resistance component at all frequencies. For the frequencies of interest, between 0.2 to 1.2 cps, this feed system is almost entirely resistive; that is, the feed-system impedance vector falls within the shaded area and has a magnitude R_F.

With the constant pressure exit condition, a feed-system-coupled instability would be expected to occur if, at some frequency, R_F is equal to or less than the boiler negative resistance R_B. The net resistance in the system would then be

either zero or negative at that frequency. Examination of the two curves within the shaded regions shows that this is possible at a frequency of about 0.48 cps.

It was possible to experimentally verify the validity of this stability criterion with the boiler dynamics test rig itself. In this frequency range, R_F was determined primarily by the hydraulic resistance of the controllable throttle valve. Normally R_F was larger than R_B, so that the net resistance was positive and the system was normally stable. Now, with the valve oscillating device turned off, it was possible to gradually open the valve beyond its normal set point and decrease R_F. When R_F became equal to or slightly smaller than R_B, the system spontaneously went into natural oscillation as shown by the flow and pressure traces of figure 2-22. The frequency of the natural oscillation was 0.48 cps, which agrees with the predicted frequency. Also, the pressure lags the flow by 180^o; that is, the pressure oscillation is at a minimum when the flow oscillation is at a maximum indicating that there is indeed a negative-resistance condition at this frequency.

Further, as the experiment demonstrates, this type of instability can be avoided by providing sufficient feed-system hydraulic resistance close to the boiler inlet. And, there is a means of deciding how large this resistance must be. In a practical system, the feed-system resistance can be made sufficiently large by providing orifices at the inlet to the boiler tubes, for example.

This discussion has been mostly about single-tube boilers. However, the same principles apply to individual tubes fed from a header in a multitube heat exchanger boiler as well as to a parallel bundle of boiler tubes coupling as a unit with the feed system.

TURBINE EROSION

A problem common to nonorganic Rankine system turbines is the blade erosion that results from liquid impingement. The NASA is investigating, both analytically and experimentally, the turbine blade erosion problem in its liquid metal systems as a consequence of the erosion experienced in steam turbines. It is recognized that the efficiency of the Rankine system can be improved by expanding the vapor in the turbine to the lowest possible pressure and temperature. But, this condition is accompanied by increased moisture content in the latter turbine states. It is in these latter wet stages that liquid impact erosion becomes a serious problem. In a current potassium Rankine system under study at NASA the exit moisture would be approximately 20 percent if no moisture separation or reduction devices were provided in the turbine.

The droplet formation in the latter stages of the turbine is examined to obtain a

physical picture of some of the major elements involved in the liquid impact erosion problem. For orientation purposes, figure 2-23 shows a cross section of a typical low-pressure split spool steam turbine. The steam flow enters at the center and is expanded equally in both spools. A portion of the last-stage stator and rotor blades of this turbine is shown in figure 2-24. Wet vapor from the preceding stage enters the stator blades where a small fraction of the fine condensate in the vapor collects on the stator surfaces. The fine condensate moves along the stator surfaces within the slow-moving boundary layer to form larger droplets and puddles. This liquid is eventually swept to the stator trailing edge where the drops break away. The larger drops then undergo a second breakup by the shearing action of the main vapor flow. While most of the droplets impact the rotor, it is only the larger drops, moving at or above some threshold velocity relative to the rotor, that actually erode the rotor leading edges.

The formation and the breakaway of droplets have been observed and recorded on film using the simple technique illustrated in figure 2-25 on small steam turbines. Rocketdyne, under NASA Contract NAS7-391, has prepared a number of such high-speed films in connection with the experimental work of the NASA on droplet formation and subsequent rotor material damage. In another experimental investigation, the behavior of solids under multiple liquid impacts, using a rotating wheel- and-water-jet apparatus, is being performed by Hydronautics, Inc. under NASA Contract NASw-1608.

In addition to experimental work on various aspects of turbine erosion, the NASA is also pursuing analytical investigations of the erosion problem as it applies to the liquid metal systems. Westinghouse, under NASA Contract NAS7-390, has completed a mathematical model of the liquid impact erosion process. The model is based on experimental observations and on the results of previous analytical studies of condensation in the vapor flow. A computer program, which has been written for the mathematical model, contains these major elements that contribute to the erosion process:

(1) Expansion of the vapor from the turbine inlet to condensation in the bulk vapor at the desired turbine stage

(2) Prediction of the fraction of fine condensate that collects on the stator-blade surfaces

(3) Determination of the detachment mode and breakup of the droplets in the stator wake, and a prediction of the resultant number and respective sizes of the droplets

(4) Calculation of the velocity and impingement angle of the respective droplets impacting the rotor

(5) A prediction of rotor-blade material removal for the desired service life based on the rotor-blade material erosion rate

For verification, Westinghouse applied the analysis to the ninth-stage rotor of the Yankee steam turbine. This last stage operated at an exit moisture of 15 percent and at a temperature of 97° F. At these steam conditions and a service time of 13 000 hours, the analysis predicted the following:

(1) The zone over which erosion would take place would be along the last 4 inches of the blade-tip leading edge.

(2) The maximum depth in this eroded zone would be 16 mils.

Comparing these predictions with the actual damage, as obtained from limited data reported during a field inspection of the turbine, the erosion zone extended along 2 inches of the blade tip as shown in figure 2-26, which is a sketch of a typical damaged blade. With regard to the maximum depth of erosion in the Stellite shields, 181 blades had less than 60 mils and the remaining 15 had more than 60 mils. The Stellite 6B shields on these 15 blades had to be replaced. While the predicted maximum depth of erosion was less than the observed maximum depth, the general results are encouraging in that this analysis is the first to predict quantitatively any erosion at all in a turbine. On this basis, work on improving the mathematical model is continuing, particularly in the area of predicting droplet breakup and resultant size distribution in the turbulent stator wake flow. A simplified form of the present mathematical model is being used in the design of new steam turbines to limit erosion damage while attempting to further increase turbine output.

As part of the advanced nuclear Rankine cycle space-power-system technology program, General Electric at Evendale, Ohio has been awarded several contracts to investigate experimentally erosion damage in potassium vapor turbines. Under NASA Contract NAS5-1143 General Electric ran a two-stage turbine for 5000 hours. Figure 2-27 shows the leading edges of a portion of the second-stage rotor after the test. The inlet temperature was about 1400° F, and the inlet quality to this blade row was calculated to be 96 percent. Most of the blades were fabricated from the nickel-base alloy U-700, and the remainder were from the molybdenum-base alloys TZM and TZC. No droplet impact erosion was experienced in any of the blades. This result is in agreement with the Westinghouse analytical erosion model which predicted negligible droplet formation at this moisture level.

Currently, a more severe moisture erosion test is in progress at General Electric under NASA Contract NAS3-10606. Figure 2-28 shows the rotor assembly of a three-stage turbine which is being tested at a third-stage rotor inlet temperature of about 1200° F and at a calculated quality of 90.4 percent. At the conclusion of the tests, the extent of erosion damage will be compared with the anlytically predicted values.

CAVITATION IN PUMPS

Cavitation, which is the formation and collapse of vapor within a flowing system, occurs in regions of pump blading where a combination of low ambient pressure and high local velocities are obtained. In a region of high velocity, if the static pressure drops below the vapor pressure of the liquid, vapor bubbles are formed. As these bubbles move with the flow to regions of higher pressure they can collapse violently.

Cavitation is a problem in a pump for two reasons. The implosions of collapsing bubbles can damage the pump blading or casing. Also, when cavitation is severe it can disrupt the flow through the pump, and thus performance is affected adversely.

The effect of increasing cavitation on the performance of a pump is illustrated in figure 2-29, where pump pressure rise for a given speed and flow is shown to depend on the margin of inlet pressure above the vapor pressure or net positive suction head (NPSH). The point of cavitation initiation occurs at a pressure well above that for which performance is affected. At this point it already produces noise and can be detected with a stethoscope on the pump casing. When vapor forming on the pump blade surfaces caused the flow to separate from the blades, the pump output deteriorates rapidly. Large vapor formations are present in the pump when this performance curve becomes vertical.

The flow in an axial flow pump rotor operating in water is shown in figure 2-30. Cavitation-free flow, moderate cavitation at the point of performance dropoff, and extensive cavitation associated with a large performance loss are illustrated in figures 2-30(a), (b), and (c), respectively. With moderate cavitation (fig. 2-30(b)) where the pump operated just above the point of severe performance falloff, both blade-tip cavitation and suction-surface cavitation are evident. Although the blade-tip cavitation is quite prominent, it had no appreciable effect on pump-blade performance. As inlet pressure was reduced, blade-surface cavitation continued to grow (see fig. 2-30(c)). With this large amount of vapor present on the suction surface, the pump no longer operated effectively.

Photographs of the cavitation formations in a centrifugal pump were taken with the camera oriented as indicated in figure 2-31. A typical illustration of cavitation is shown in figure 2-32. These photographs of cavitation were taken in pump rotors that might be used in turbopumps for rocket engines where cavitation damage is not a problem because the duration of engine operation is so short. However, cavitation damage is a problem in the pumps for a turbogenerator electric power system, which must operate reliably for long periods of time. In this case, liquid sodium or potassium may be the working fluid. Since it is not economical to subcool the

condensate, it must be pumped by the condensate return pump in a near-boiling condition. Cavitation damage in this pump is the primary concern.

The problem is evident from the cavitation damage observed on a mixed-flow impeller which was tested at the Pratt & Whitney CANEL installation in liquid potassium at 1400° F for 350 hours. The mixed-flow impeller shown in figure 2-33 is about 7 inches in diameter. The damage (fig. 2-34) occurred on the rear surface of the blade near the trailing edge. The severe pitting would have been followed shortly by blade failure. Some of the pits are 1/16 inch in depth.

Cavitation damage occurs on a fluid-containment surface, such as a pump blade, where adjacent vapor cavities rapidly collapse. Although various studies have shown that pure vaporous cavities can collapse rapidly and at high energy levels, the basic mechanics of damage by imploding vapor bubbles is not clearly established. Recent research, however, has revealed one way in which cavitation damage occurs. Figure 2-35 shows the successive phases of an imploding cavitation bubble near a solid surface. Figure 2-35(a) shows a cavitation bubble adjacent to a surface somewhat as it would appear moving along the suction surface of a pump blade. As the bubble moves into a zone of higher pressure, the vapors within condense rapidly, and the collapsing bubble takes odd shapes. As a bubble collapses (figs. 2-35(b), (c), and (d)), a jet of liquid is formed, which pierces the bubble and impinges on a small area of the adjacent blade surface. The center of the jet appears in the photographs as a dark core which extends above the bubble.

Lewis Research Center has sponsored research on materials that resist cavitation damage. Studies of cavitation damage with the use of alkali-metal pumps are supplemented by work with a magnetostrictive vibratory device which closely simulates pump-blade damage. This device (fig. 2-36) consists of two principal parts - a magnetostrictive vibrator, and a test specimen that is driven by the vibrator. Cavitation damage is produced on the surface of the 0.5-inch-diameter circular specimen, which is submerged in liquid and caused to vibrate at high frequency. On each upstroke vapor bubbles are formed near the surface of the specimen. These bubbles collapse with high energy on the ensuing downstroke. The device provides a practical method for making rapid, accurate, and detailed measurements of the rate of weight loss for a given material.

The cavitation erosion rates for a number of materials, tested over a range of conditions, are presented in figures 2-37 and 2-38. The curves for 304-L stainless steel and 316 stainless steel are similar in that the damage rate is small initially, rises sharply, and then falls off to a constant steady-state zone. The damage rate differs for the various materials. In water, for example, soft aluminum is eroded by cavitation about 60 times faster than stainless steel. The resistance of several refractory alloys - TZM, T-222, and columbium 132M - has been

studied in liquid sodium. These alloys maintain their strength at the high temperature of interest in space-power systems. In 400° F sodium, the resistance of these materials to cavitation damage (based on steady-state values) is comparable with that of 316 stainless steel. Stellite 6B, a cobalt-base alloy, is remarkably resistant to damage. After 14 hours of exposure, weight loss was only beginning to become measurable. Because of its high cost and the difficulty of fabrication, it is impractical to fabricate an entire pump rotor of Stellite. An inlay of Stellite in the most damage-prone area of the blading, however, might greatly extend pump life.

In order to determine which physical properties of the material are important in determining the resistance to cavitation damage, it is important to consider the mechanism of damage. Basically, the containment material is exposed to the jet impingement and pressure shock waves of imploding bubbles on or very near its surface. Damage resistance, then, is a measure of the capacity of a material to absorb this mechanical attack before fracture or pitting occurs. Thus, high values of yield strength, ultimate tensile strength, hardness, and ductility (percentage of elongation to fracture) are beneficial in providing resistance to cavitation damage.

In space-power systems, operation at high-temperature levels is desirable; thus, it is important to consider the effect of fluid temperature on the rate of cavitation damage. The rate of damage for three materials immersed in liquid sodium at 400°, 1000°, and 1500° F are compared in figure 2-39. All the data presented were obtained with the liquid sodium at atmospheric pressure. The greatly reduced rate of damage observed at 1500° F occurs despite the fact that the specimen materials have less strength at this higher temperature.

The decreasing damage at higher temperatures is caused by a change in the properties of the liquid and vapor. To understand the process, the flow in the passage between two pump blades as illustrated in figure 2-40 is considered. A cavitation bubble forms near the suction or low-pressure surface of one blade. This bubble is then swept across the passage to the surface of the adjacent blade where the pressure is higher. There must be a violent, rapid collapse of the bubble close to the blade surface to cause damage.

At relatively low temperature, as in room temperature water, the rate of bubble collapse is limited only by the inertia of the liquid surrounding the bubble. At higher temperatures closer to the boiling point, however, the rate of bubble collapse is controlled by thermal limitations - the rate at which the saturated vapor within the cavity can be condensed on the surrounding liquid interface.

The vapor pressure of sodium as a function of temperature is plotted in figure 2-41. The curve rises steeply at higher temperatures. Bubble collapse is slower and therefore less damaging at high temperatures for two reasons. First, the density of the saturated vapor in the bubble is proportional to vapor pressure.

Thus, a given size bubble will contain a greater mass of vapor at high temperature. The greater mass of vapor takes a longer time to condense. Also, condensation is a heat-transfer process. As a bubble moves across the passage it goes through a pressure change ΔP. Initially the bubble is filled with saturated vapor at the temperature of the surrounding liquid. In the high-pressure region the temperature of the saturated vapor inside the bubble is greater than that of the surrounding liquid by the condensing ΔT (fig. 2-41). At the higher temperature, because of the greater slope of the curve, the ΔT corresponding to the same pressure difference is much smaller. This lower ΔT reduces the rate of condensation and contributes to a slower bubble collapse.

These two effects - a greater mass of vapor in the bubble and the smaller temperature difference between the vapor and the ambient liquid - combine to cause a much slower bubble collapse and therefore less damage at high temperature. At the high temperature of operation of space-power systems, about 1500° F, damage rates are so low that some pump cavitation may be tolerable. However, at temperatures of about 1000° F sodium shows a cavitation damage rate comparable to that of room temperature water. It will probably be necessary, therefore, to operate the sodium pumps in stationary powerplants at a pressure level and flow condition for which cavitation is avoided.

HIGH-TEMPERATURE LIQUID METAL PUMPS

The utility companies use, almost exclusively, the submerged pump for liquid metal service. These pumps, using conventional motors, have overall efficiencies of over 80 percent. They do, however, require a dynamic seal between the motor and the liquid metal cover gas. Space-power high-temperature liquid metal loops cannot tolerate any contaminants, and this has required the development of totally sealed pumps.

Two types of liquid metal pumps being developed are the canned motor pump and the electromagnetic or EM pump. An example of the canned motor pump is the SNAP-8 sodium-potassium (NaK) pump shown in figure 2-42. The pump and a 400-cycle motor are mounted on one shaft and are wholly contained within a welded housing. The pump inlet and exit are welded into the liquid metal loop forming a single, completely sealed unit. No shaft seals are required since both pump and motor are submerged in the same NaK fluid. The high-temperature pumped NaK is separated from the cooler NaK in the motor cavity by a short annular thermal barrier. The pivoted pad journal bearings and double acting pivoted-pad thrust bearings are also lubricated and cooled by cavity fluid. To protect the electrical ma-

terials from chemical attack by the liquid metal, both rotor and stator are encapsulated within welded Inconel cylinders or "cans."

This pump delivers 100 gallons per minute of NaK at an overall efficiency of 35 percent. The low efficiency is due to the small size of the rotor and the presence of the Inconel cans.

One of these units recently completed over 10 000 hours of trouble-free operation. The endurance test included over 800 scheduled start-stop cycles, attesting to the physical integrity of the bearing pads and ball pivots. While the motor hot-spot temperature was maintained at 450° F, the electrical materials used are designed for 1000° F hot-spot service. If this high-temperature material technology is used, a canned motor pump might be developed for sodium service without the need for an external cooling system.

The electromagnetic pump is simpler in concept than the canned motor pump in that the EM pump has no moving parts. Because of the EM pump's simplicity, and despite its lower efficiency, it provides liquid metal systems the maximum in pumping reliability for long duration, unattended space missions. A cross section of a helical induction pump is shown in figure 2-43.

The liquid metal enters the pump at the right into an annular passage. The helical induction EM pump is analogous to an induction motor except that the rotor has been replaced by a liquid metal filled annular passage. The rotating magnetic field imparts a force on the liquid causing it to rotate circumferentially in the annulus. Since the fluid is constrained to flow within the helical channel in the annulus, the fluid moves from one end of the pump to the other. At the same time, the fluid static pressure increases along the helical channel. The high-pressure fluid makes a 180° turn at the end of the annulus and exits the pump at the right through the center pipe. With both fluid connections at the same end of the pump, the stator and cooling passages can be removed, if necessary, without disturbing the sealed liquid metal loop.

NASA has contracted with the General Electric Company to develop a boiler feed pump of the type shown in figure 2-43. The pump is being designed to deliver 33 gallons per minute of potassium at 1000° F. The pump has a calculated efficiency of 18 percent. The stator hot-spot temperature will be limited to 1200° F by using a potassium coolant. All the electrical materials used in the pump, except for the stator end turn connections, have been successfully tested to 1300° F for 10 000 hours. This pump is now in the final stages of assembly, preparatory to testing.

In spite of the lower efficiencies, the canned motor and electromagnetic pumps may provide highly reliable, long-life service for secondary applications in central power stations.

MATERIALS

The current SNAP-8 boiler, described previously, utilizes tantalum as the mercury containment material because of its excellent corrosion resistance and 316 stainless steel as the heating fluid containment material. During the early part of the SNAP-8 development program, however, extensive use was made of 9Cr-1Mo steel throughout the system including the boiler. This material (most often referred to as Croloy 9M or Sicromo 9M) is commonly used in steam systems, primarily in the reheaters.

As the SNAP-8 program progressed, a change was made to a material developed by the Timken Roller Bearing Company called modified 9M, which was considerably stronger than the standard alloy. The improved strength was achieved primarily by a slight chemistry modification and also by a 1900^{o} F normalize and 1350^{o} F temper heat treatment. The chemistry modification consisted of the addition of very small amounts of columbium, vanadium, boron, nitrogen, and zirconium (the total elemental addition being less than 1/2 of 1 percent).

The improved strength properties are clearly illustrated in figure 2-44 in which modified 9M in the normalized and tempered condition is compared with standard 9M, 304 stainless steel, and 315 stainless steel (all in the annealed condition). Plotted is the ASME Boiler and Pressure Vessel Code maximum allowable stress values for each material against temperature. The 321 stainless steel would fall below but near the 316 stainless steel. There are no code values for modified 9M at this time; however, the curve shown was constructed using the same ground rules under which the curves for the other materials were constructed (i.e., 1/4 ultimate tensile strength and 60 percent of 100 000-hr rupture strength). Over the temperature range shown, the modified 9M is much stronger than 9M, stronger than 304 stainless steel, and is stronger than 316 stainless steel up to at least 1100^{o} F. The material has indicated no instabilities even after approximately 18 000 hours of stress rupture testing at 1100^{o} F.

A thorough welding study of the material was conducted at Lewis Research Center. No noticeable difference between it and the standard 9M was observed. The material requires a postweld heat treatment, just as do 9M and the other low and medium chrome steels. As is the case with standard 9M, the material can be utilized up to about 1300^{o} F without excessive scaling.

Because of the improved strength of the modified alloy, it could be used in reheaters in place of 9M. Being able to use a considerably thinner wall would result in a significant cost saving.

The modified alloy could also be used in high-pressure superheater applications in place of 304, 321, 347, or even 316 stainless steel at the same wall thickness if

the postweld stress relief does not impose significant constraints. The cost savings in this case would be very significant as shown in figure 2-45. There is a factor of 2 between modified 9M and 304 stainless steel, a factor of $2\frac{1}{2}$ between it and 321 stainless steel, and a factor of >3 between it and 316 stainless steel.

As noted, the modified 9M has already been used in SNAP-8 boilers. It has also been used in a high-temperature conveyor application. It is likely there are many applications where it could be substituted for more costly materials currently being used.

Stellite 6B, a cobalt-base alloy, is commonly used as blade shielding in the final stages of steam turbines. The use temperature is normally less than 200° F. Stellite 6B has also been considered for service in other areas in steam turbines. One such area is as the nozzle block material for the first stages where significant erosion has been observed in some installations. The temperature in these areas can be as high as 900° to 1100° F, and because of these higher temperatures there is a need for caution based on past experience.

Stellite 6B was utilized in the SNAP-8 turbine shown in figure 2-46. This turbine is a four-stage impulse-type machine, 10 inches in diameter and 20 inches long. The Stellite was used as the nozzle-diaphragm and wheel-blade material in all four stages. It was selected since it was one of the most erosion-resistant materials known.

All available information indicated no potential danger in utilizing Stellite 6B at elevated temperatures. The first turbine, however, failed catastrophically in less than 1000 hours. Examination of the failed parts revealed extremely brittle fracture. The shattered first-stage wheel is shown in figure 2-47.

Subsequent metallurgical studies at Aerojet-General Corporation determined that the material was unstable over the entire operating temperature range of the turbine. Carbide precipitation, which increased the hardness from a normal R_c of 40 to as high as 50 was found to occur. There was also a tendency toward transformation of the crystal structure from face centered cubic (FCC) to hexagonal close packed (HCP) accompanied by a volume decrease. These metallurgical changes resulted in a significant decrease in the material's ductility and resistance to impact. The two hardness extremes are compared in figure 2-48 in terms of the tensile elongation as a function of temperature.

The upper curve is representative of the condition in which the material would normally be put into service. The lower curve is representative of the condition of the material after thermal aging in service occurs. A turbine designer would not utilize a material of such low ductility if he knew about it in the beginning.

A comparison of the impact strengths of the original and thermally aged material is shown in the following table:

Hardness, Rockwell C	Crystal structure	Impact strength, ft-lb
40	FCC	4.2
50	HCP	1.2

Only relative values are important since subsize specimens were used. The R_c 50 material in the HCP crystal structure had approximately one-third the impact strength of the R_c 40 material in the FCC crystal structure.

The metallurgical study also showed that some lots of Stellite 6B were considerably more stable than others. It was determined that the stability of a given lot of material depended on its chemistry, prior processing history, and prior heat treatment. As a result of the study, however, Stellite 6B was eliminated as the SNAP-8 turbine material.

The foregoing does not entirely rule out Stellite 6B for elevated temperature service. It does, however, caution potential users to test thoroughly, at the service temperature, the particular lot or lots of material planned to be used. This would be particularly true if the material is to be exposed to mechanical or thermal shock or both.

COMPUTER SIMULATION OF SYSTEM DYNAMICS

A previous discussion treated some dynamic problems that involve one or two components of the powerplant. Some aspects of boiler stability and dynamic coupling of the boiler with its feed system were discussed. It was shown that sometimes a relatively simple mathematical analysis can indicate the way to avoid trouble. However, there are other dynamic problems that involve all the components of the powerplant. Here the mathematical analysis is much more complicated. Therefore, these system dynamic problems are studied by simulating the powerplant with a computer.

Computer simulation, of course, is not new. It has been used widely in both industry and government in recent years. Therefore, this discussion does not dwell, to any extent, on the techniques involved in puting a simulation together or on the mathematical methods used. Instead, the discussion is focused on a particular application in which a computer simulation was very useful.

This application was in the development of an automatic startup system for the

space powerplant shown schematically in figure 2-49. This is the SNAP-8 system, which is currently being developed. It is a three-loop nuclear Rankine powerplant with mercury as the fluid in the vapor loop. When this system is put into space, the entire startup will be controlled by an electrical programmer. The design of this programmer required detailed information on the startup transients. In obtaining this information, extensive use was made of a computer simulation of the powerplant.

The type of computer simulation used to study the startup transients is illustrated in figure 2-50. The computer depicted in this figure is a large-capacity general-purpose one. The input information includes the many equations that represent the individual components of the powerplant. It also includes the computing logic that provides for the component interactions of the real system. The role of the computer is to take over the big job of solving the many equations. The output of the computer, of course, is the system information. The startup transients can be displayed in the form of tables or graphs. Plots of variables against time are especially convenient, since they are usually recorded in this manner during startups of the actual system.

The advantage of the large-capacity computer was that it simplified the job of writing the component equations. Because the computer was able to handle many equations, the complicated components were subdivided into parts that were easy to analyze. As mentioned previously, the mathematical analysis will not be discussed in detail. However, it should be pointed out that this approach of subdividing complicated components does give good results. The reactor was one component treated in this way. In simulating the reactor, three basic subdivisions were used - control, nucleonics, and heat transfer. The heat-transfer part was broken down into 22 segments.

The reactor model was compared with test data. An example comparison is shown in figure 2-51. The data were obtained from the North American Rockwell Corporation who is the developer of the reactor. For the testing, the operation of the reactor was disturbed by making step increases and step decreases in coolant flow rate. The disturbances were 500 seconds apart. The same disturbing function was imposed on the computer model. The resultant response of the nuclear power is shown: the solid curve is for the real reactor, and the dashed curve is for the computer model. The maximum difference between the curves is about 1/2 percent of the average power level.

The startup procedures for the SNAP-8 system are somewhat similar to the startup procedures used for ground-based powerplants. The main difference is that injection starting of the vapor loop is used. This is done because of the zero-

gravity environment in space. With no gravity force available, the boiler feed pump has no suction head until a sufficient pressure builds up in the condenser. Therefore, the mercury pump cannot be used in the initial startup of the boiler and turbine. Instead, during startup the initial feed rate needed by the boiler is supplied by injection from a pressurized external reservoir (see fig. 2-49). The mercury pump has to take over the job of feeding the boiler when the injection process ends. As stated before, the computer simulation was a valuable tool in defining these startup procedures and the required controls. One startup problem worked out with the computer simulation was to find the proper feed rate schedules for the injection of mercury into the loop.

This problem can be explained with the aid of figure 2-52 where some results are plotted from two different computer runs. The solid curves are for one run, and the dashed curves are for the other run. Three variables are shown for the first 3 minutes of the vapor-loop startup. They are reactor exit temperature, turbine speed, and boiler feed rate. The boiler feed rate schedules were the input variables for the two runs.

The shaded area under the solid plot of the boiler feed rate represents the amount of mercury to be injected into the loop. If this amount was injected with the rapid schedule shown, then the turbine was accelerated to its rated speed of 12 000 rpm well before the injection process stopped. The arrow on the speed curve marks the end of injection. This boiler feed rate schedule, however, resulted in critical rates of change of reactor temperature. The slope of the solid reactor temperature curve exceeds the allowable value at the point indicated. This problem could be corrected by injecting the same amount of mercury over a longer period of time. For this slower injection, the boiler feed rate schedule shown by the dashed line was used. The resulting satisfactory response of reactor temperature is shown by the dashed curve.

However, there was now another problem. With this slower schedule of boiler feed rate, the turbine acceleration was much slower, as shown by the dashed curve for turbine speed. In fact, the turbine was considerably below its rated speed at the time injection was finished; this time is marked by the arrow on the dashed speed curve. Therefore, the speed of the boiler feed pump, which was driven by the turbine generator, was also well below its rated value, and the pump could not deliver enough flow to sustain the operation after injection was over. Therefore, the turbine speed came down as shown in the figure, and the system failed to start.

With the computer, however, many boiler feed rate schedules could be studied. Eventually, schedules within these extremes were found that accelerated the turbine

and at the same time gave satisfactory reactor temperature transients.

As yet the complete SNAP-8 system has not been tested. However, there have been test versions of SNAP-8 which included everything but the reactor and the radiator. One such version used a gas-fired heat source and rejected its waste heat in an air-cooled heat exchanger. Startup tests were made with this system in which the flight-type procedures were followed as far as possible. Therefore, data from these tests were used to check the computer simulation. In doing this, of course, it was necessary to make some changes in the computer program in order to have it represent the system tested.

Some comparisons between computer results and test data are shown in figure 2-53. All parts of this figure represent the same startup run. Several of the more interesting variables are displayed for the first 10 minutes of the vapor-loop startup transient. The injection process began at time zero, and the end of the injection process is indicated by the vertical dashed lines.

The boiler feed rate schedule used in the test run and programmed into the computer is shown in this figure. The turbine speed and the temperature of the heating fluid leaving the boiler are also shown. In a complete SNAP-8 system, this would be the temperature transient fed toward the reactor. The other transients shown - the boiler exit pressure (on the vapor side of the boiler), the generator power, and the liquid weight in the condenser - were simulated quite well with the computer. The largest errors were in the latter part of the boiler temperature transient and in the generator power transient. The generator simulation was optimistic by about 10 kilowatts.

In general, the agreement between the computer results and the test data is good. Since these transients represent some of the most critical events of the startup, it can be concluded that a computer simulation can be used with confidence in the analysis of startup transients. It should also be mentioned that system transients involved in shutdown and load-following operations can also be studied advantageously with a computer simulation.

A computer simulation of a powerplant is a useful tool in designing controls and establishing operating procedures for large-excursion transients, such as startup. A computer simulation is also useful in defining emergency procedures, since many things can be tried that would be too hazardous in a real system. In addition, a computer simulation can be used to generate information pertaining to the structural requirements of the system and its components during off-design operation. The use of a computer simulation as a training aid for powerplant operators should also be considered. A training simulator much like the ones used to train pilots or astronauts could be set up by means of computer simulation.

SUMMARY

The discussion of Rankine power conversion system technology has touched upon a variety of topics. It is evident that potential economics in once-through boiler size, weight, and cost can be realized by the improvement of heat flux associated with the use of internal flow control inserts that separate the liquid and vapor phases within the boiler tubes. Space-power-system boilers using swirl inserts have been built and tested, and the results verify the applicability of the technology to the design of compact boilers.

A scheme for incorporating double containment within the boiler component was described. Boilers utilizing this concept have been built and operated and they have proven effective in avoiding operational hazards associated with the intermixing of boiling and heating fluids in reactor-powered systems.

The boiling instability phenomena were characterized. In general, the attenuation or elimination of instabilities requires identification of the type of instability and then making appropriate adjustments of the operating variables having influence on the particular instability encountered. Experimentally verified analytical techniques for predicting boiling instabilities are effective tools for guiding the thermodynamic and fluid dynamic design of boilers and coupling requirements of the boiler feed system.

The progress toward the understanding of the turbine blade erosion mechanisms and the analytical modeling of the process for purposes of predicting erosion damage rates has been reviewed.

The consequences of pump cavitation in terms of structural damage to the pump impeller and pump performance were discussed in some detail. Although adequate net positive suction head (NPSH) can normally be maintained in ground-based systems to avoid cavitation, there are distinct pump impeller materials choices to be made to provide added insurance against premature pump failure from cavitation damage.

Two types of high-temperature pump designs were described. These concepts, while having lower efficiencies than the more commonly used submerged pumps, provide compact noncontaminating units for special applications.

The virtues of a modified 9Cr-1Mo steel were examined relative to other materials commonly used in power systems with a view toward the economics of system or component construction. The results, though still rather preliminary, are encouraging. Since caution is necessary when using Stellite 6B at elevated temperatures, the user should thoroughly understand the characteristics of the particular lot of material to be used.

The value of computer simulation for the analysis of system transient behavior was described briefly. The technique provides a means for definition of complete system dynamics over a much broader range of conditions than could safely be attempted with the actual system as well as the definition of efficient and safe-operating procedures and the establishment of effective control logic. Furthermore, once the system is properly modeled on a computer, the simulation can be utilized for the training of operating personnel.

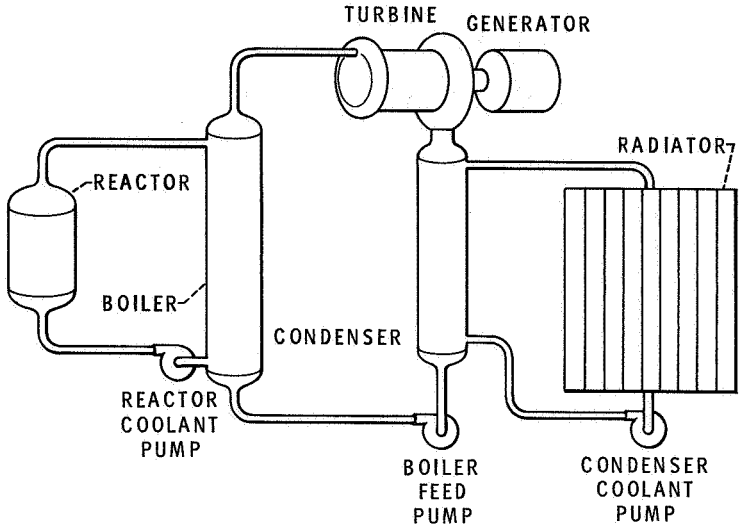

Figure 2-1. - Space nuclear power plant.

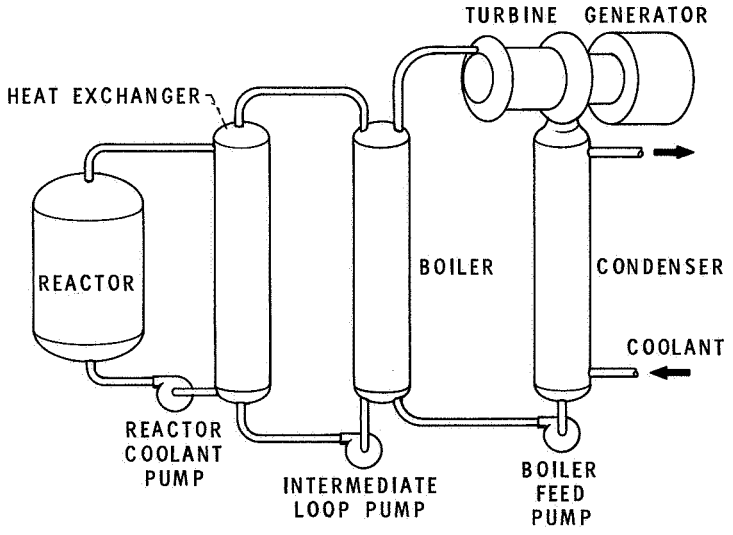

Figure 2-2. - Ground nuclear power plant.

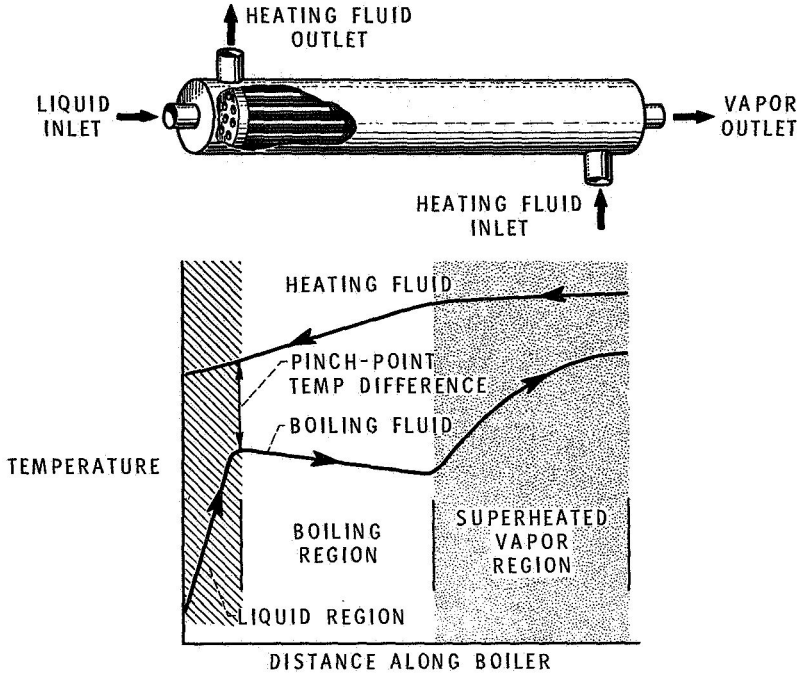

Figure 2-3. - Temperature distribution in "once-through" boilers.

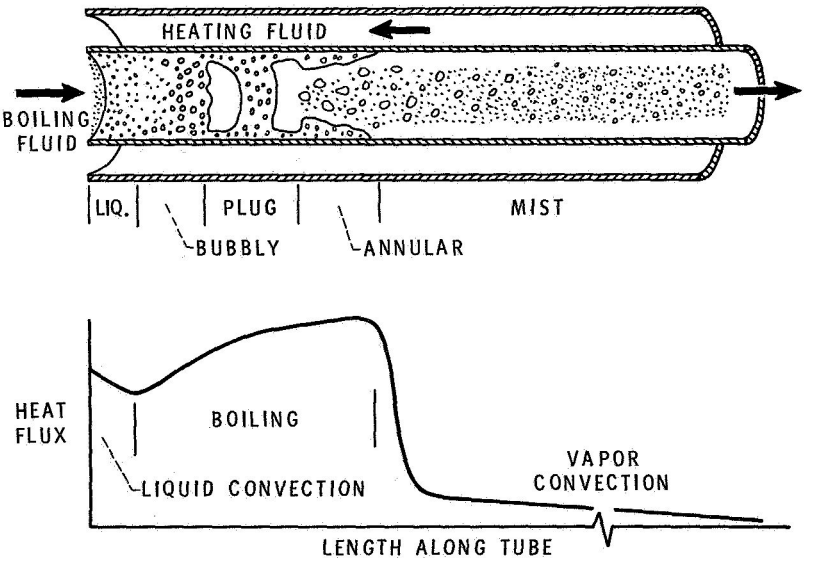

Figure 2-4. - Boiling flow regimes.

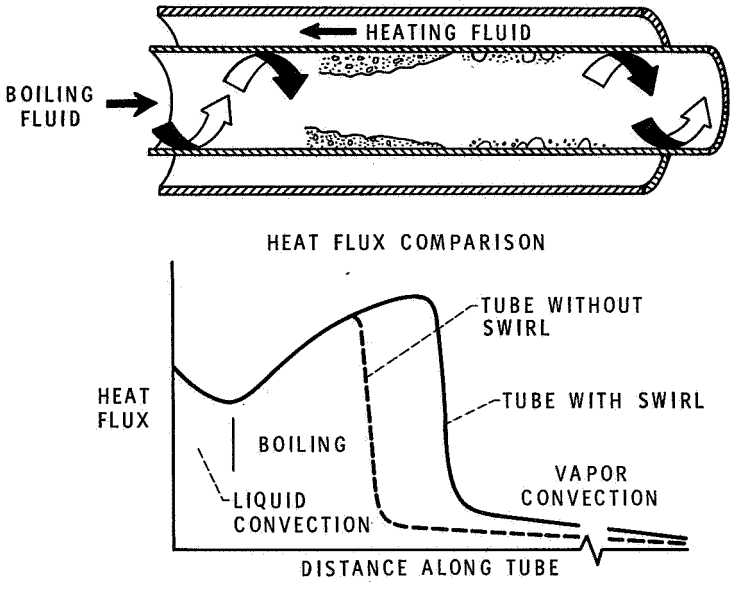

Figure 2-5. - Swirl-flow boiler concept.

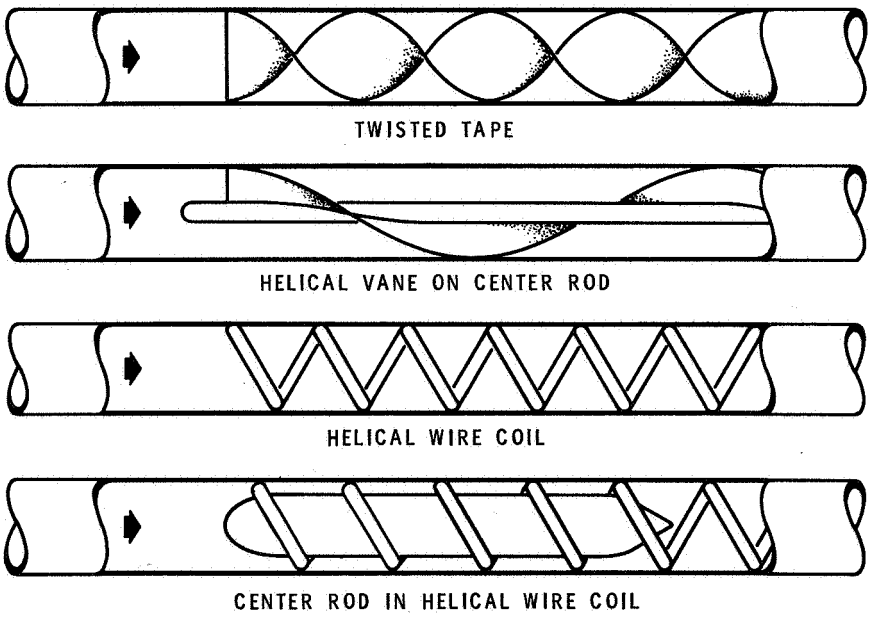

Figure 2-6. - Boiler tube inserts.

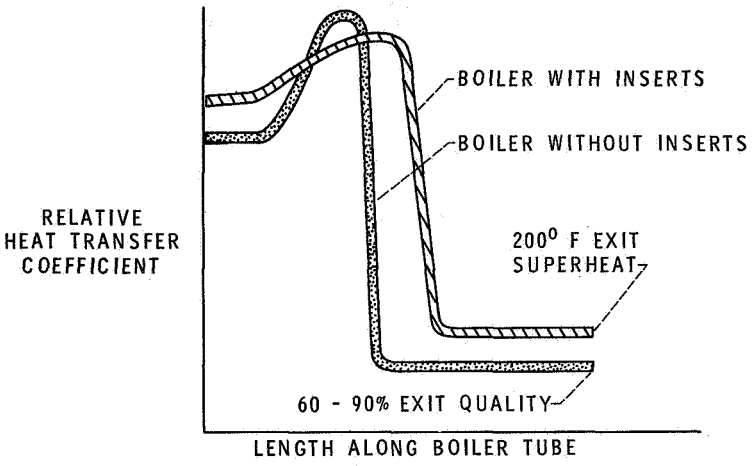

Figure 2-7. - Comparison of boiler performance.

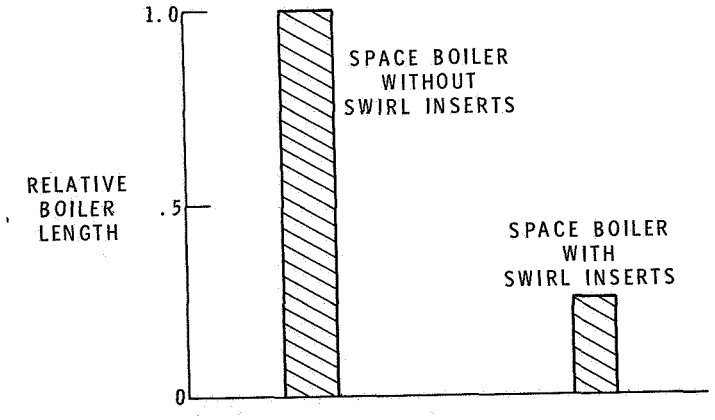

Figure 2-8. - Comparison of boiler lengths.

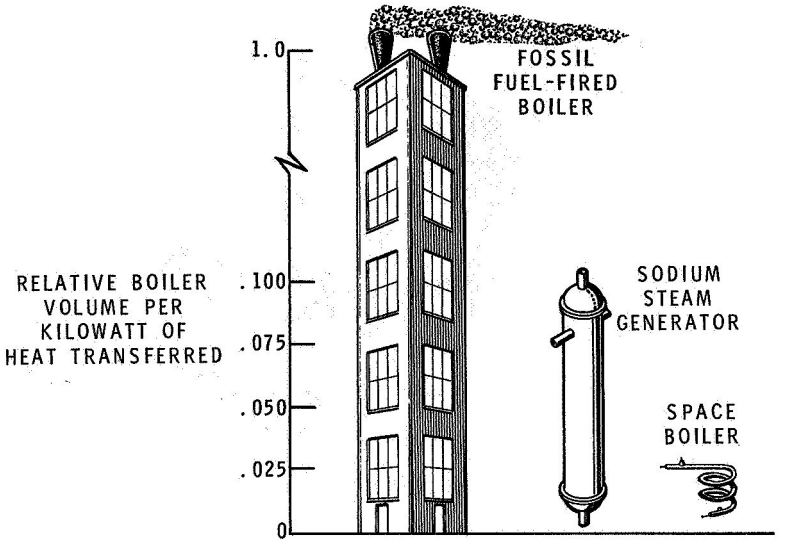

Figure 2-9. - Comparison of boiler sizes.

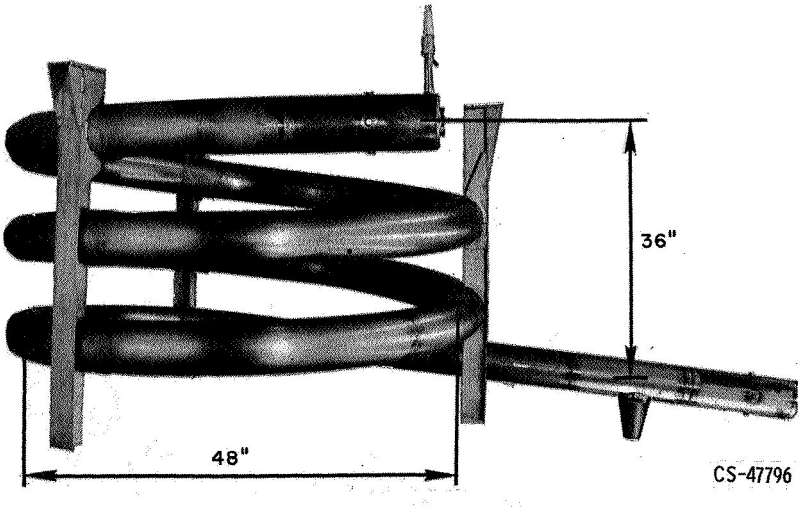

Figure 2-10. - SNAP-8 mercury boiler.

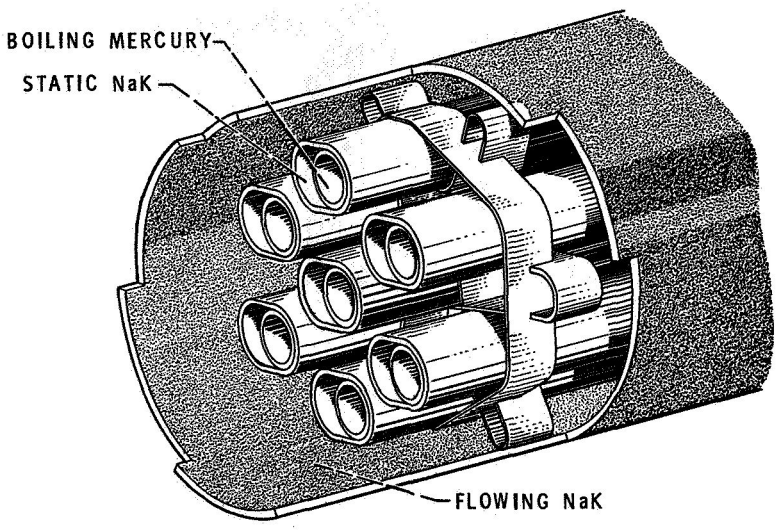

Figure 2-11. - SNAP-8 boiler tubes.

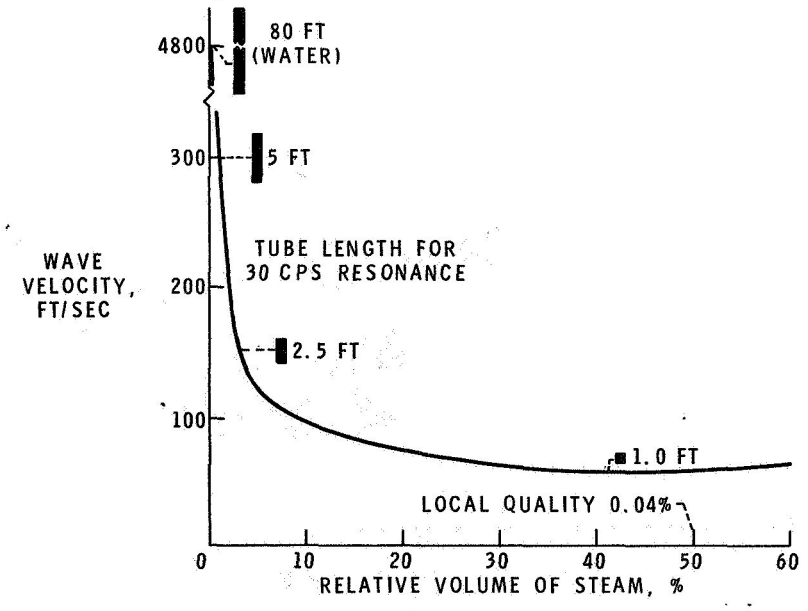

Figure 2-12. - Speed of sound for pressure of 1 atmosphere.

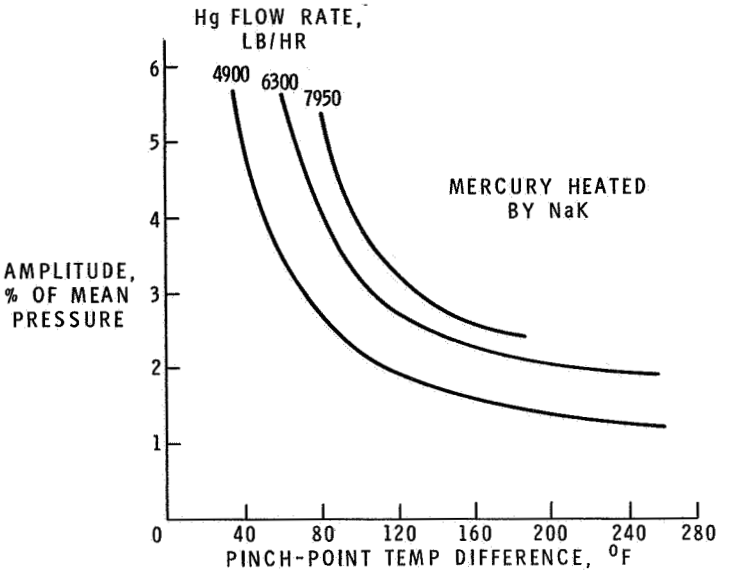

Figure 2-13. - Pinch-point effect on boiler-outlet pressure oscillations. (Mercury heated by NaK.)

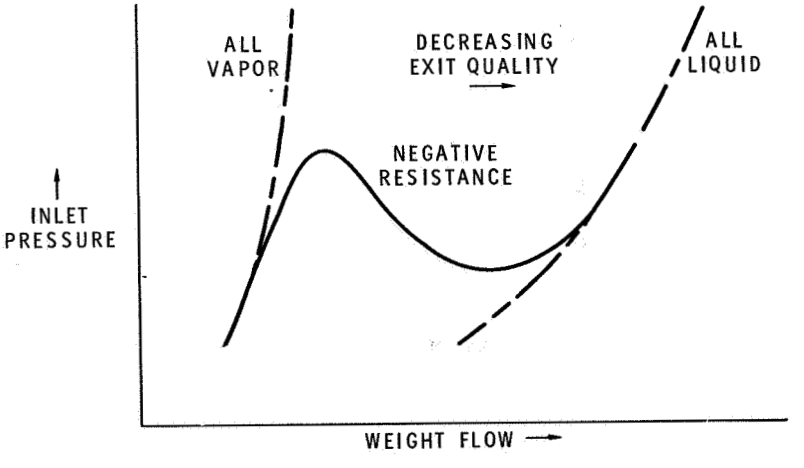

Figure 2-14. - Boiler pressure. Exit pressure constant.

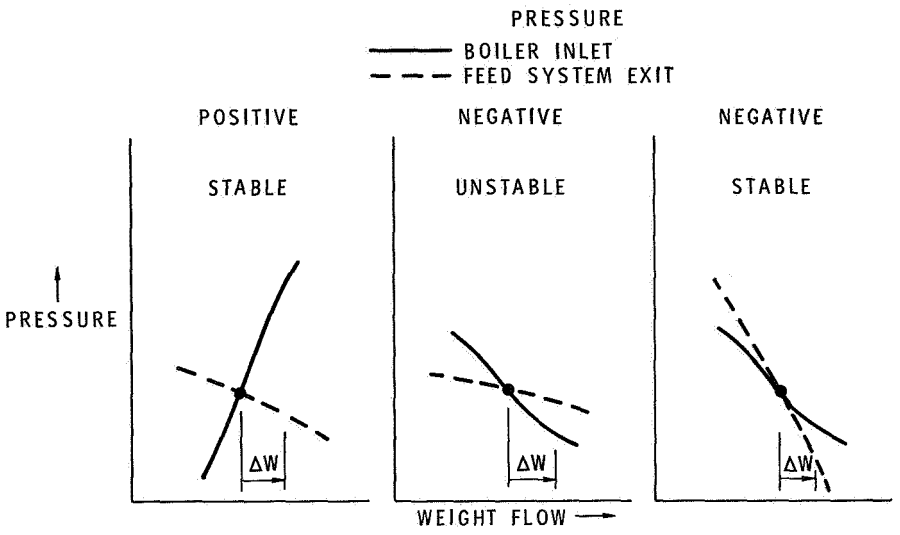

Figure 2-15. - Boiler resistance.

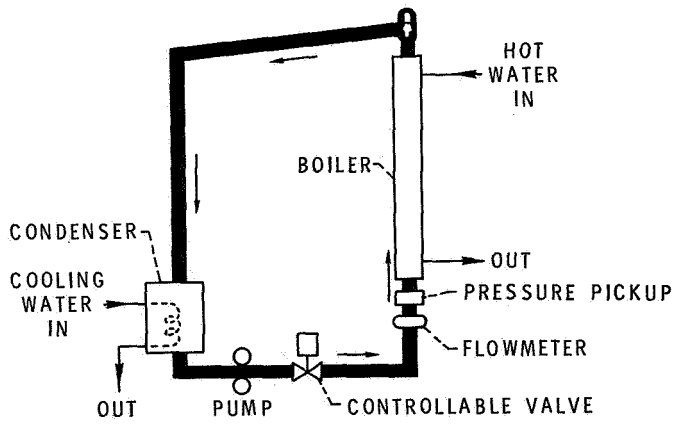

Figure 2-16. - Schematic diagram of boiling-Freon dynamics loop.

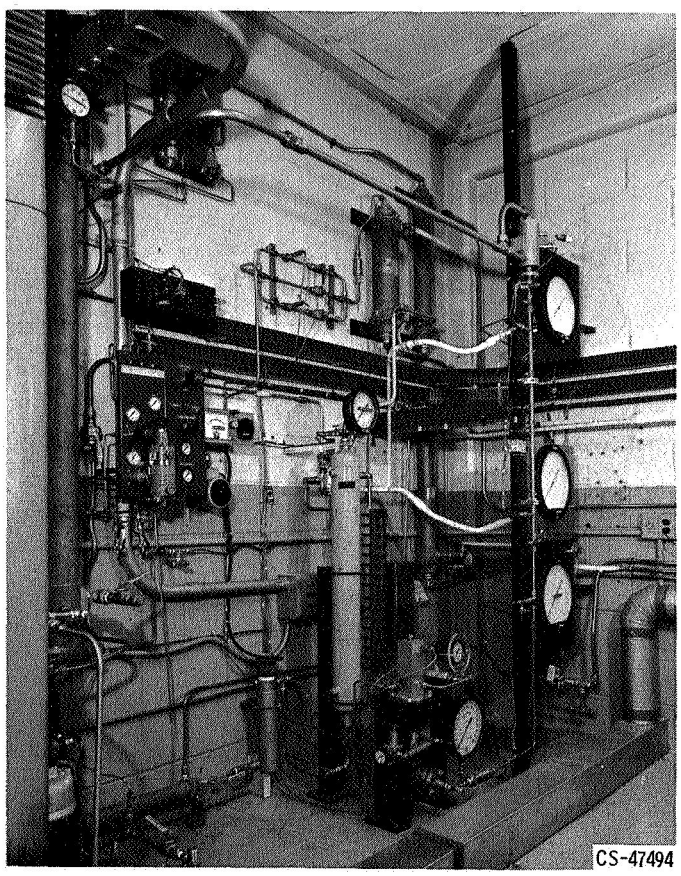

Figure 2-17. - Boiling-Freon dynamics loop.

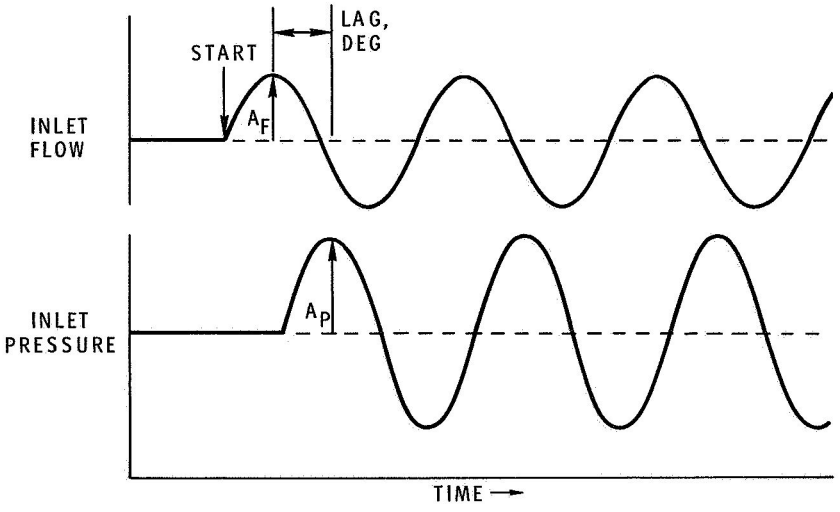

Figure 2-18. - Forced oscillations.

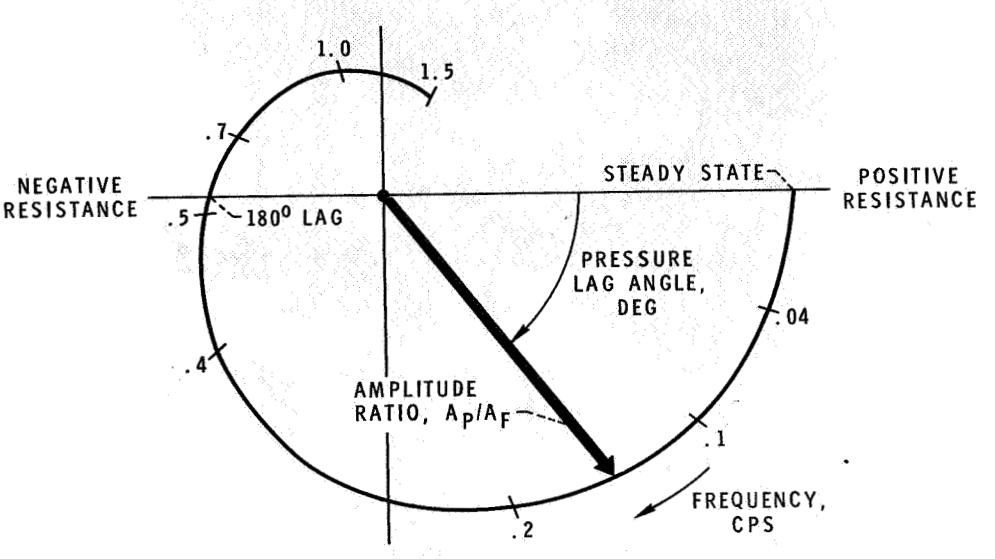

Figure 2-19. - Boiler inlet impedance in polar coordinates.

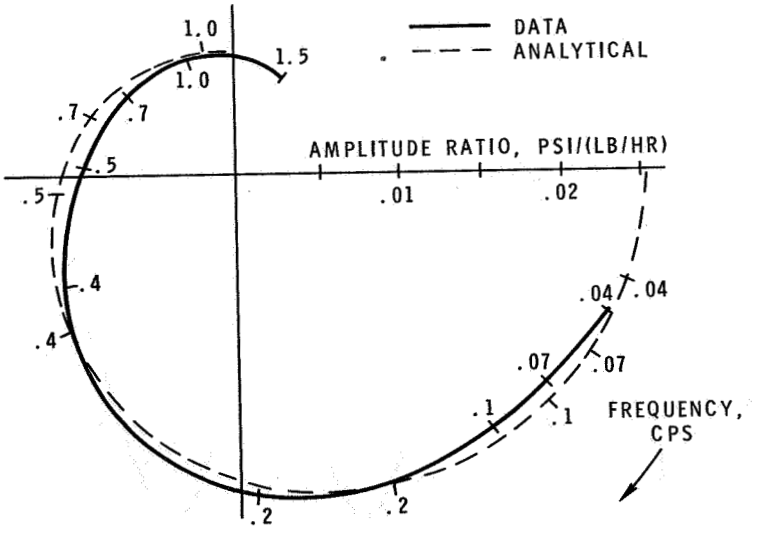

Figure 2-20. - Actual frequency response data for boiler inlet impedance.

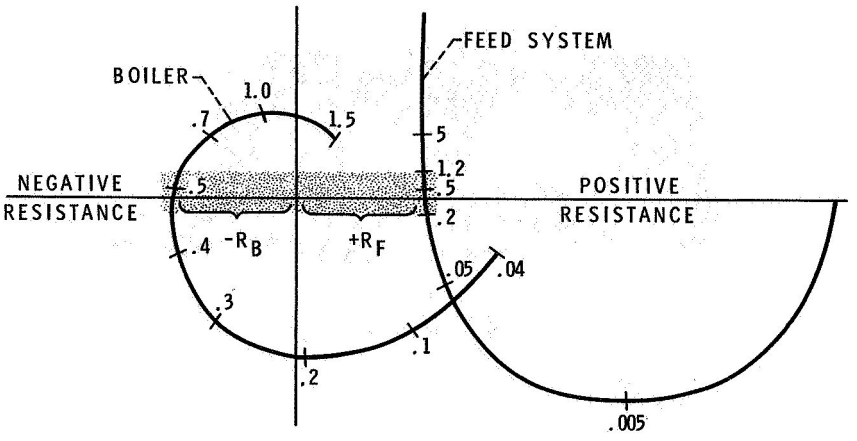

Figure 2-21. - Boiler inlet and feed-system impedances.

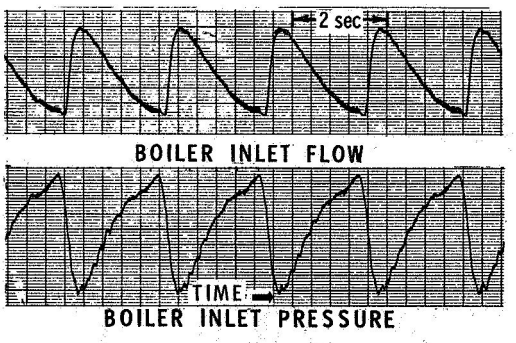

Figure 2-22. - Natural pressure and flow oscillations. Frequency, 0.48 cps; pressure lag, 180^0.

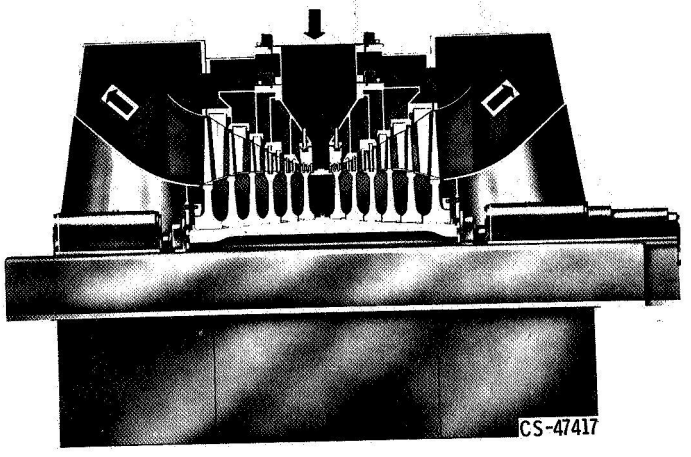

Figure 2-23. - Low-pressure turbine.

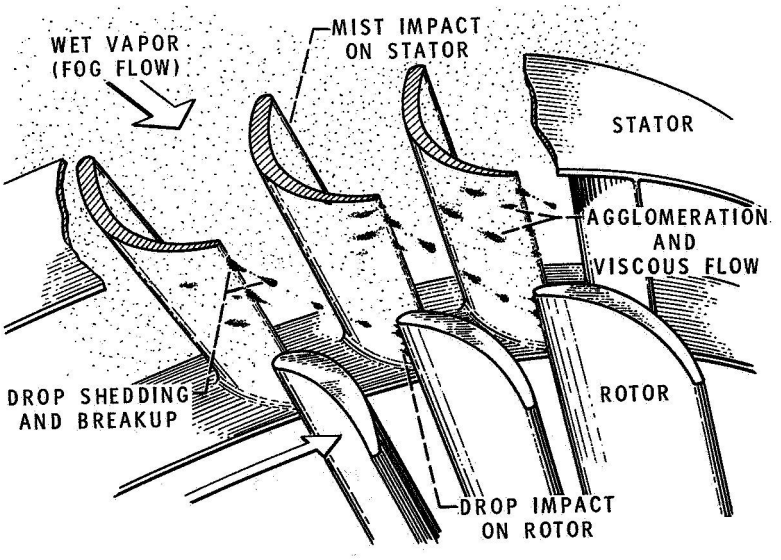

Figure 2-24. - Droplet growth and impact.

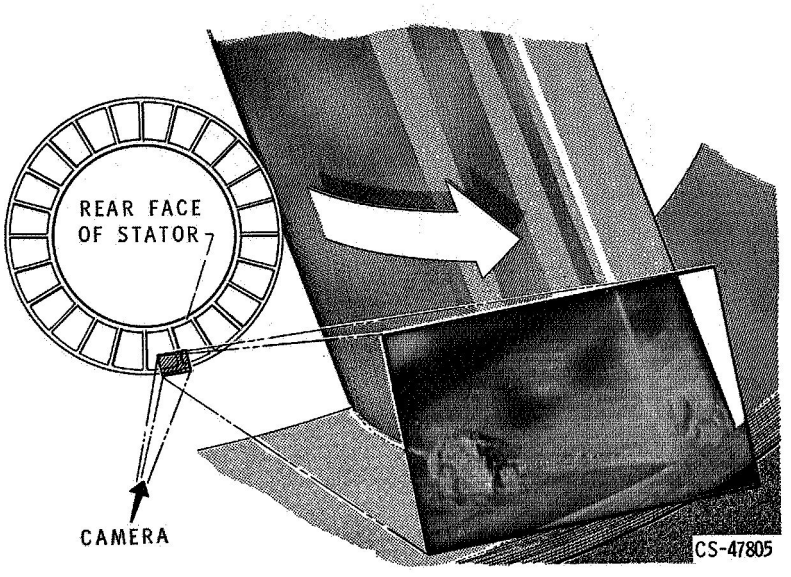

Figure 2-25. - Moisture flow visualization.

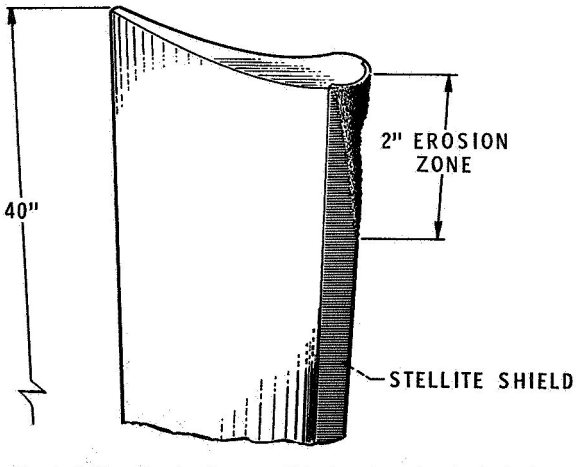

Figure 2-26. - Erosion damage of Yankee steam turbine. Ninth stage rotor after 13 000 hours; exit quality, 85 percent; temperature, 97° F.

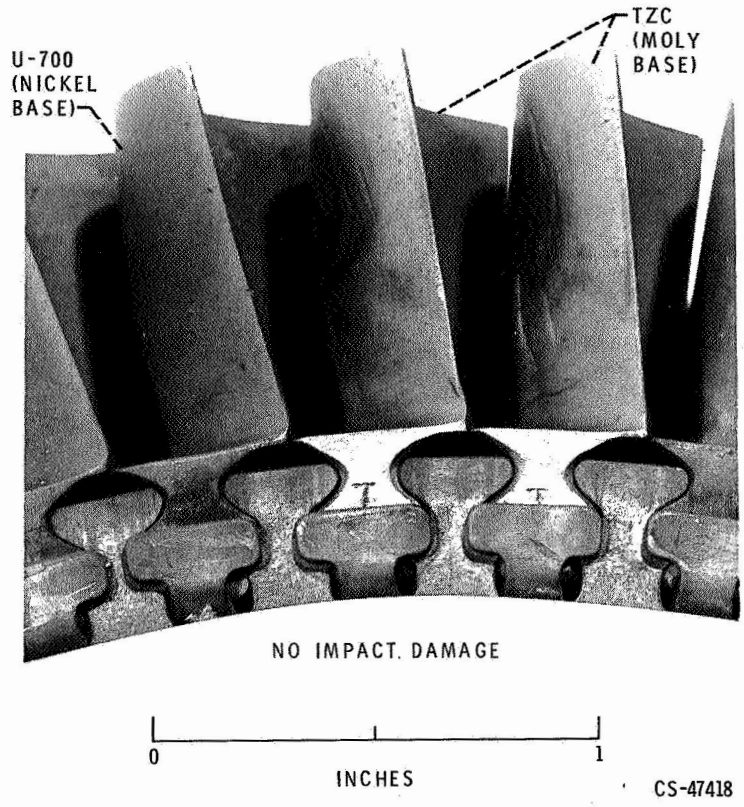

Figure 2-27. - Rotor-blade leading edge after 5000-hour test in potassium vapor. Exit quality, 92 percent.

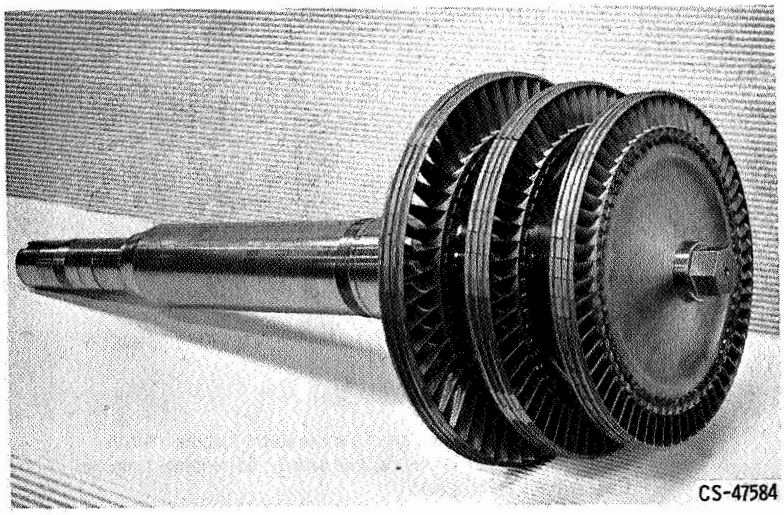

Figure 2-28. - Three-stage potassium vapor turbine rotor.

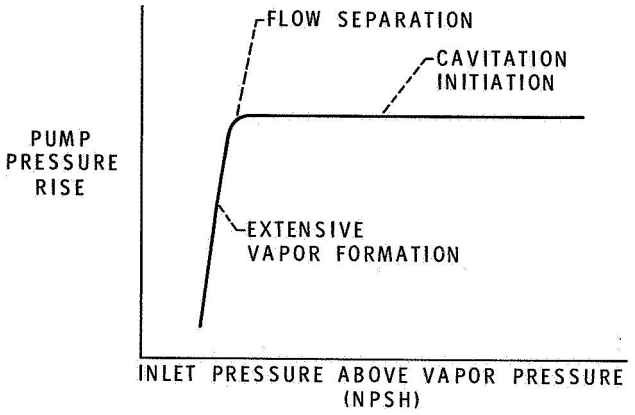

Figure 2-29. - Effect of cavitation on pump performance.

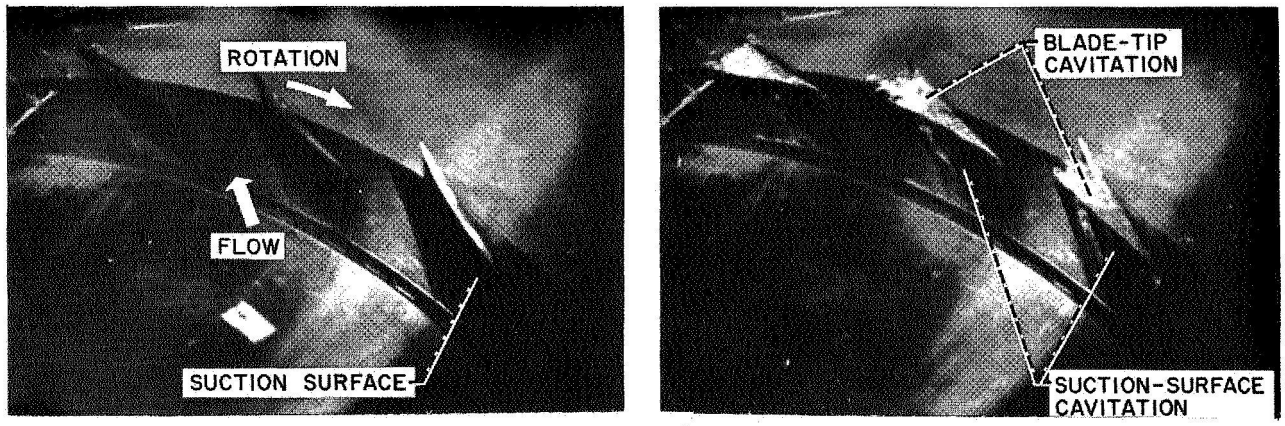

(a) No cavitation.

(b) Moderate cavitation.

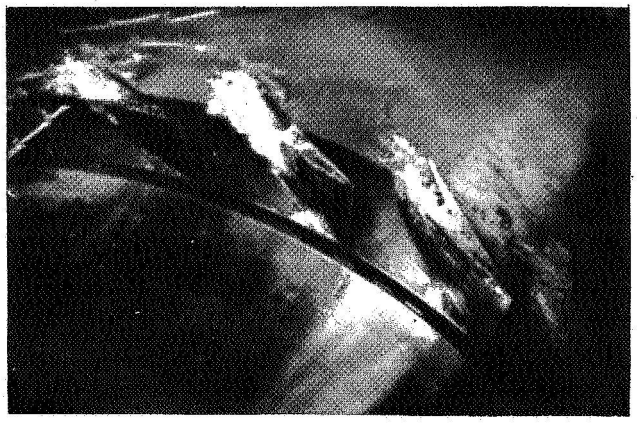

(c) Extensive cavitation.

Figure 2-30. - Axial flow pump rotor operating in water.

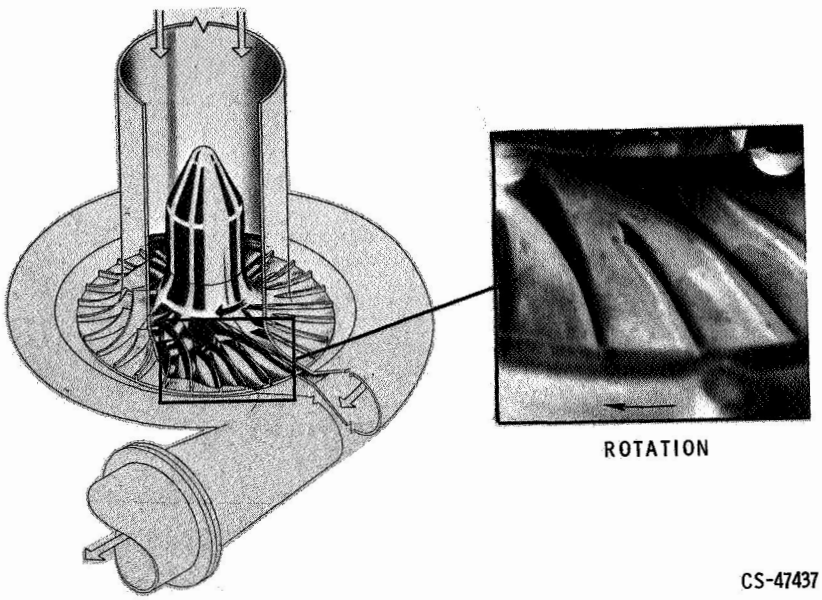

Figure 2-31. - Centrifugal pump.

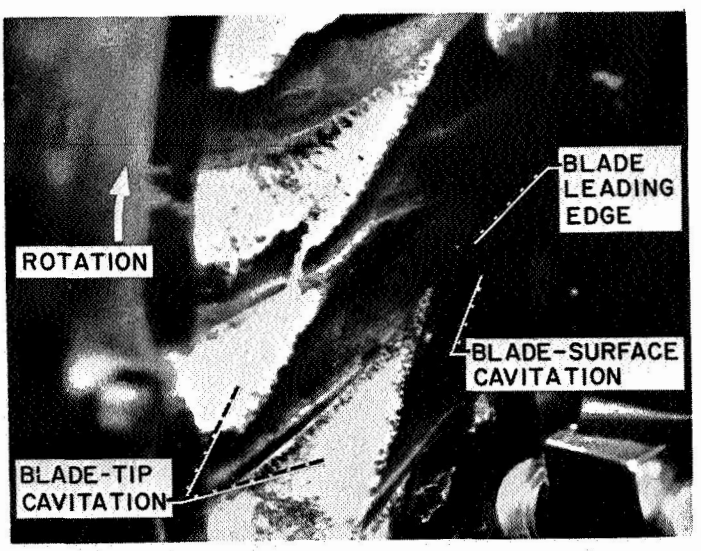

Figure 2-32. - Typical illustration of cavitation.

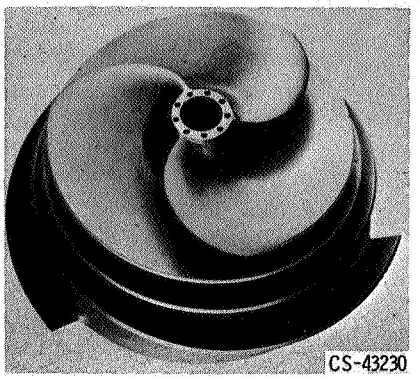

Figure 2-33. - Mixed-flow impeller for potassium tests.

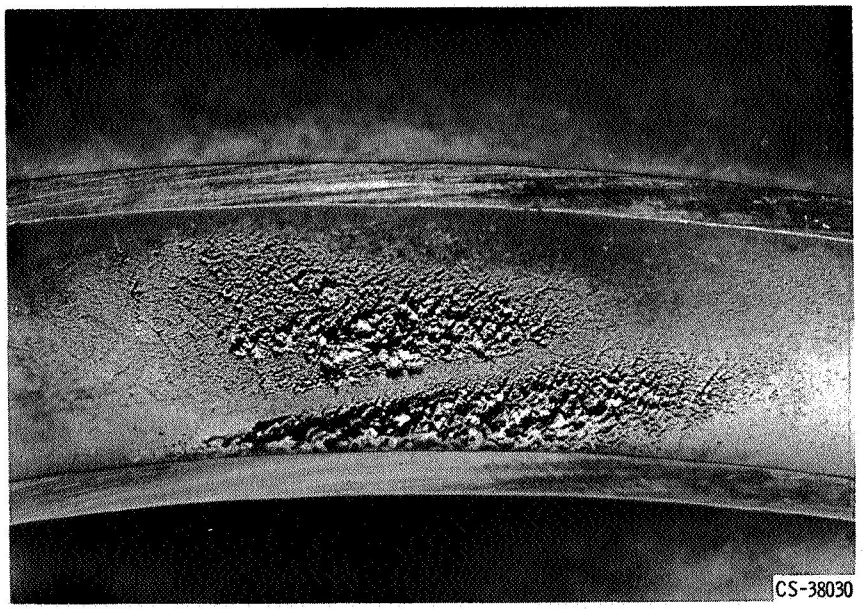

Figure 2-34. - Rotor cavitation damage.

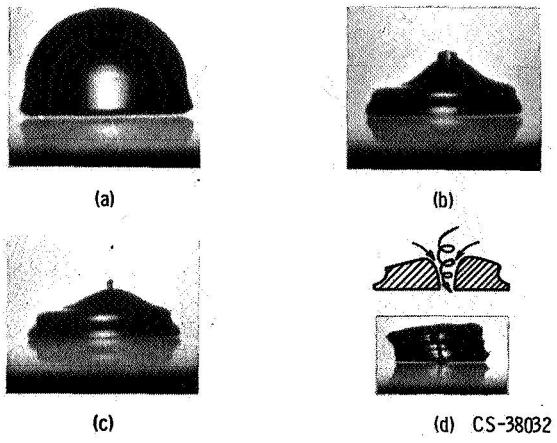

Figure 2-35. - Vapor bubble collapse mode. (Courtesy A. T. Ellis, California Inst. of Tech., and T. B. Benjamin, Univ. of Cambridge.)

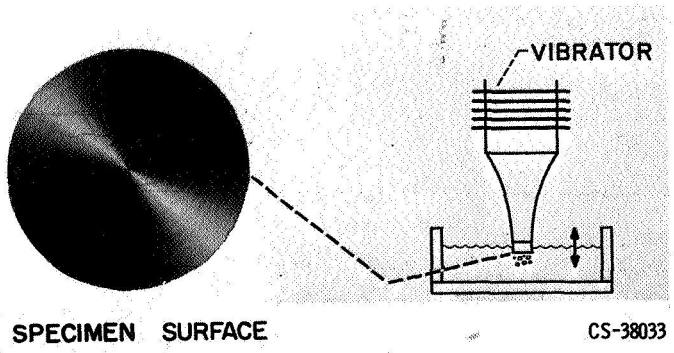

Figure 2-36. - Cavitation damage device.

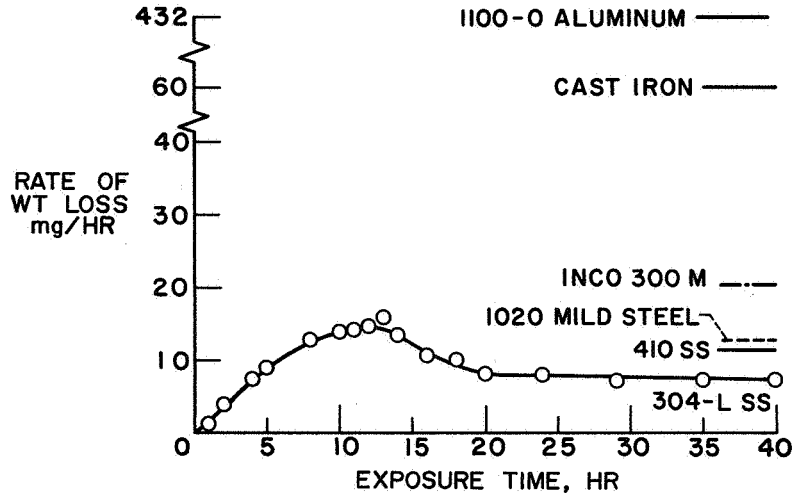

Figure 2-37. - Cavitation damage rate in 80° F water.

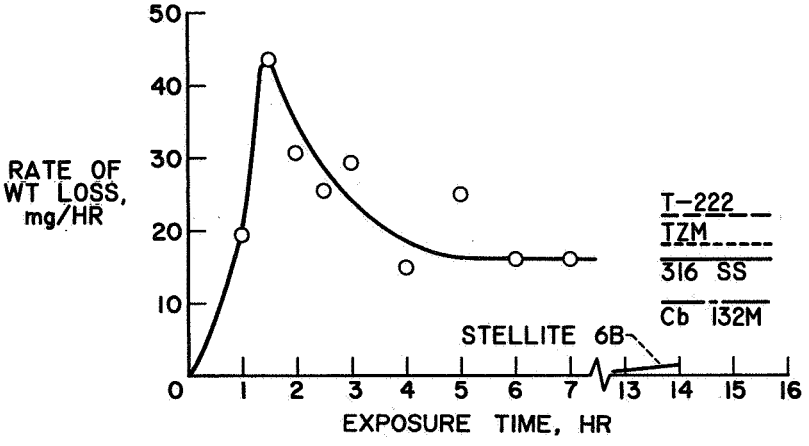

Figure 2-38. - Cavitation damage rate in 400° F liquid sodium.

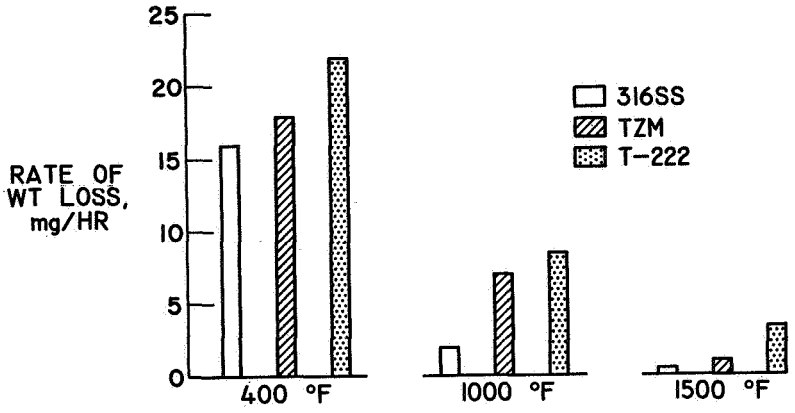

Figure 2-39. - Effect of temperature on cavitation damage rate in liquid sodium.

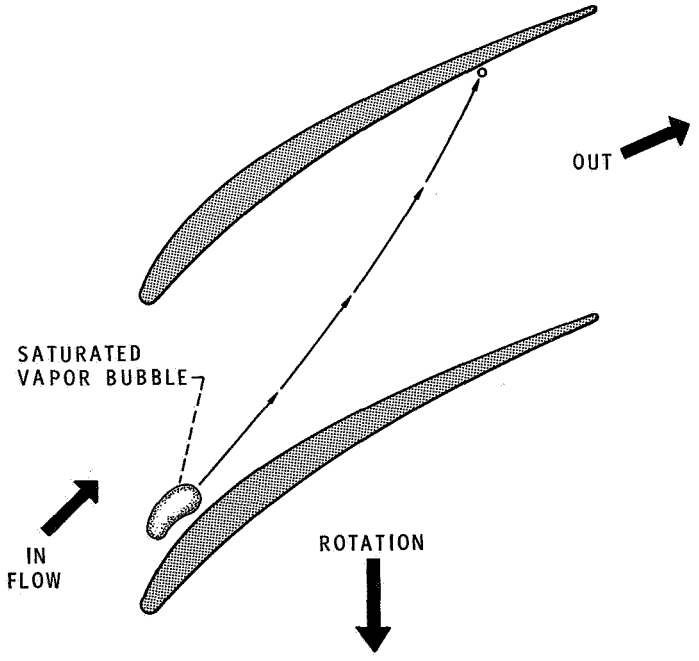

Figure 2-40. - Bubble collapse in pump.

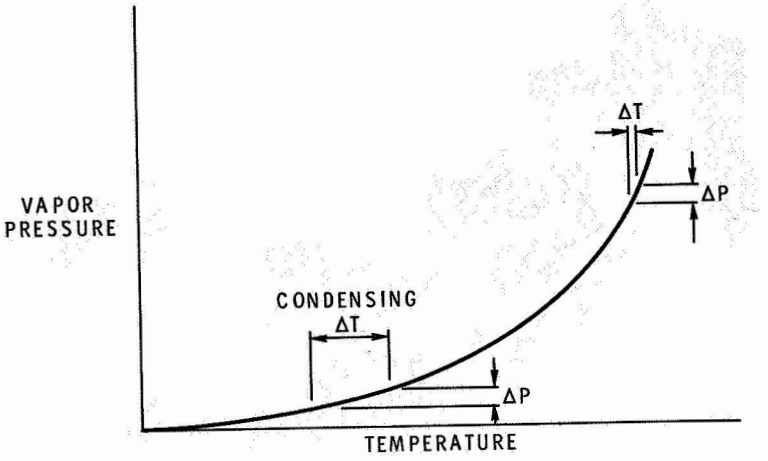

Figure 2-41. - Sodium vapor pressure.

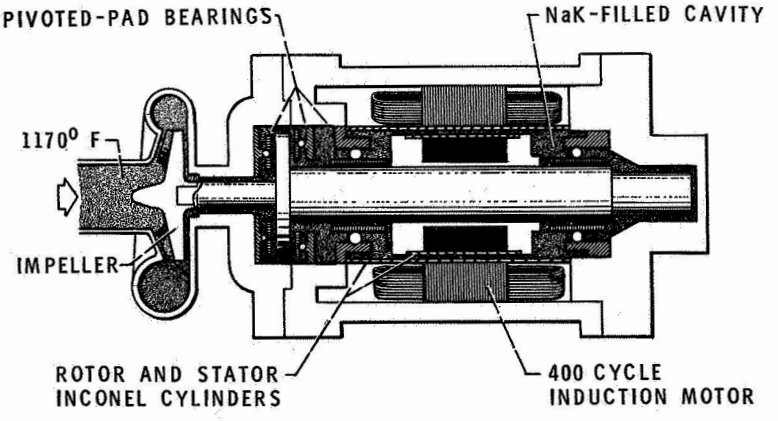

Figure 2-42. - SNAP-8 NaK pump-motor assembly.

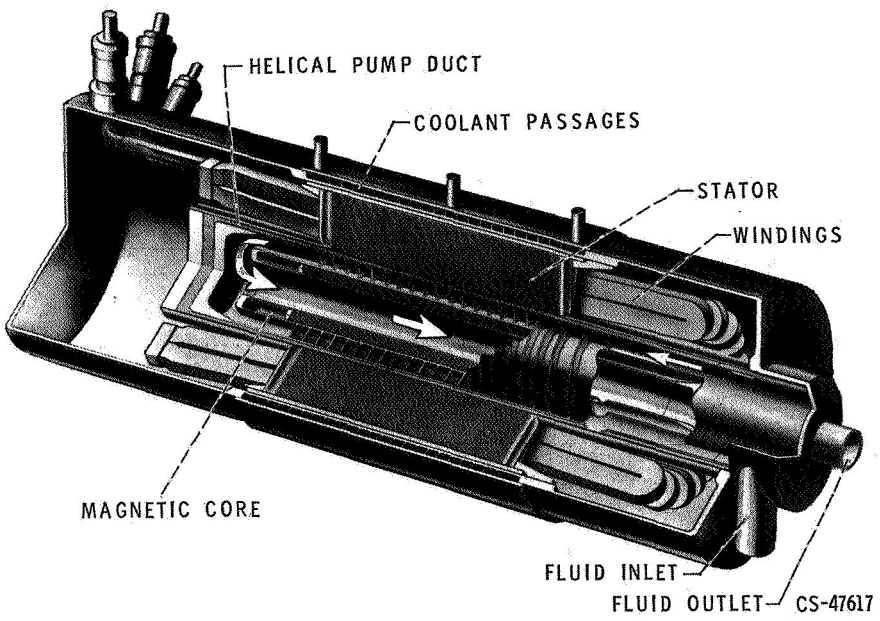

Figure 2-43. - Electromagnetic helical induction pump.

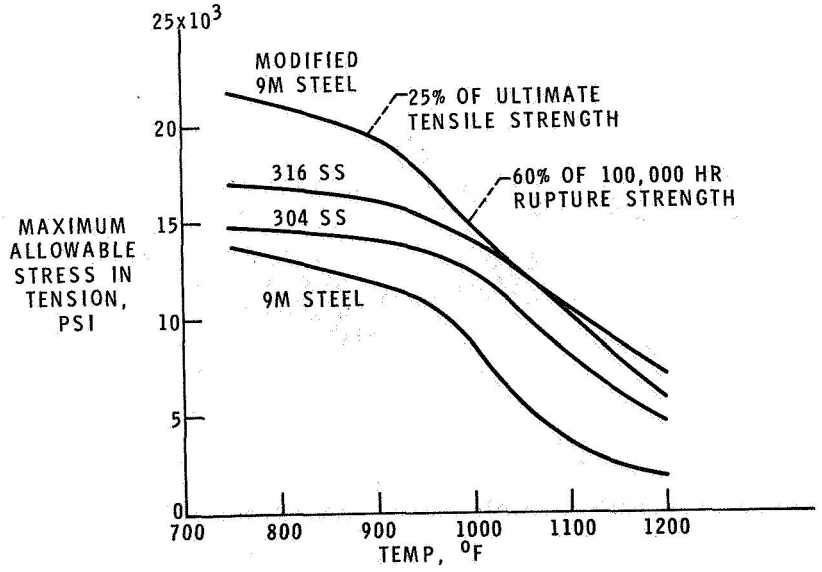

Figure 2-44. - Strength of modified 9M steel. (ASME Boiler and Pressure Vessel Code.)

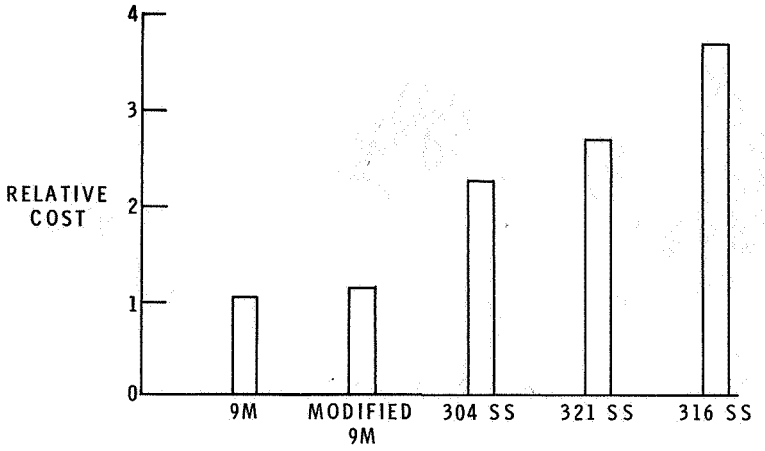

Figure 2-45. - Relative cost of tubing. Tube, 2-inch outside diameter by 0.250-inch wall.

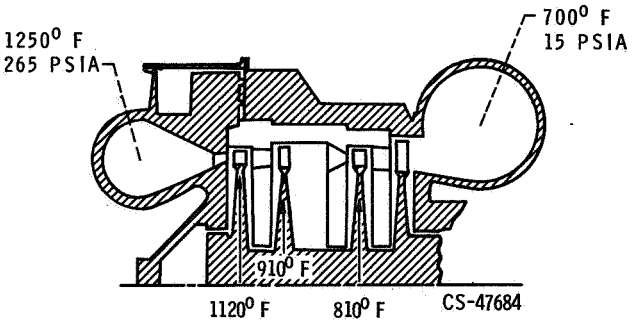

Figure 2-46. - SNAP-8 turbine.

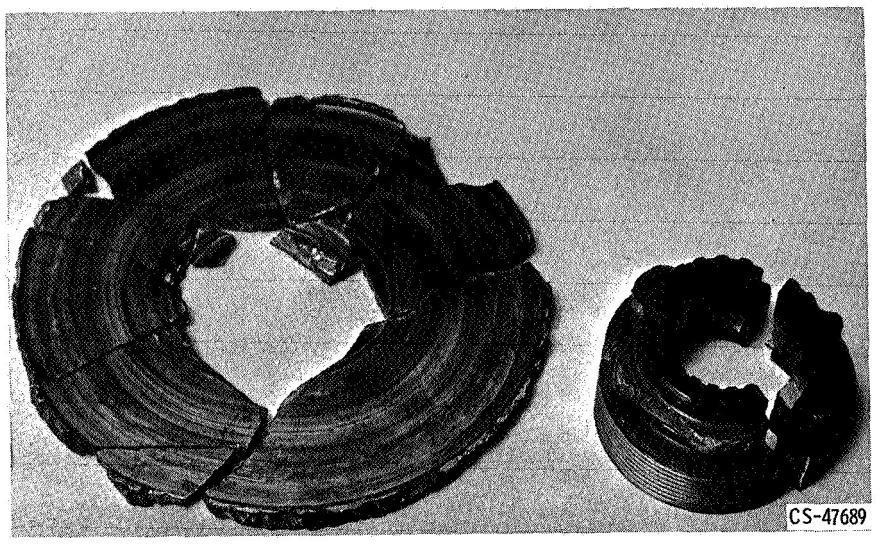

Figure 2-47. - First-stage turbine wheel.

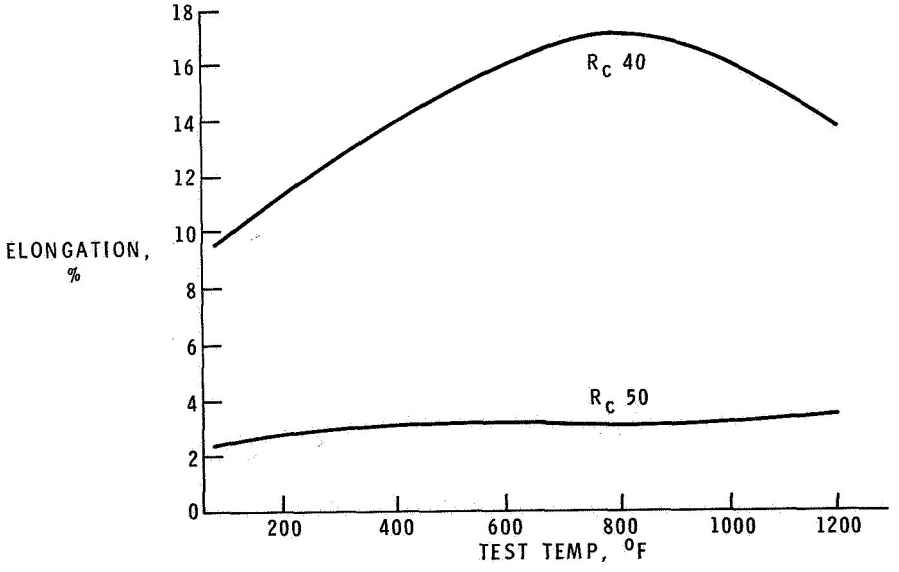

Figure 2-48. - Effect of test temperature on ductility of Stellite 6B.

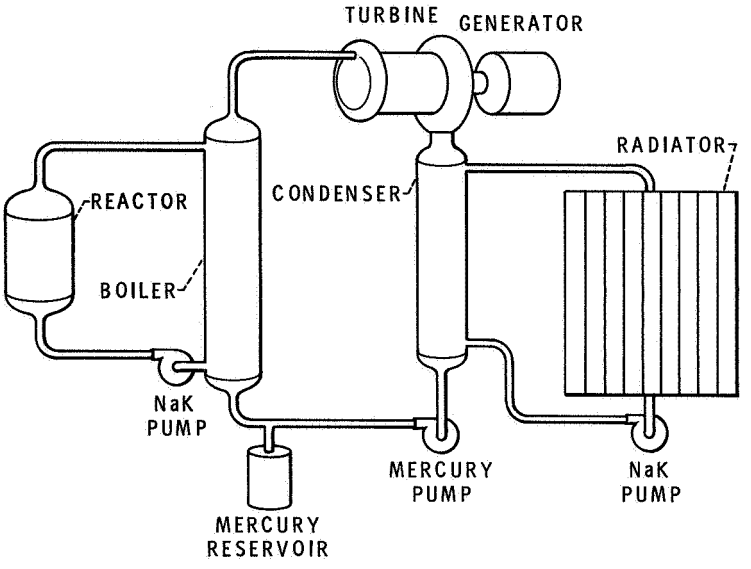

Figure 2-49. - Space nuclear powerplant (SNAP-8).

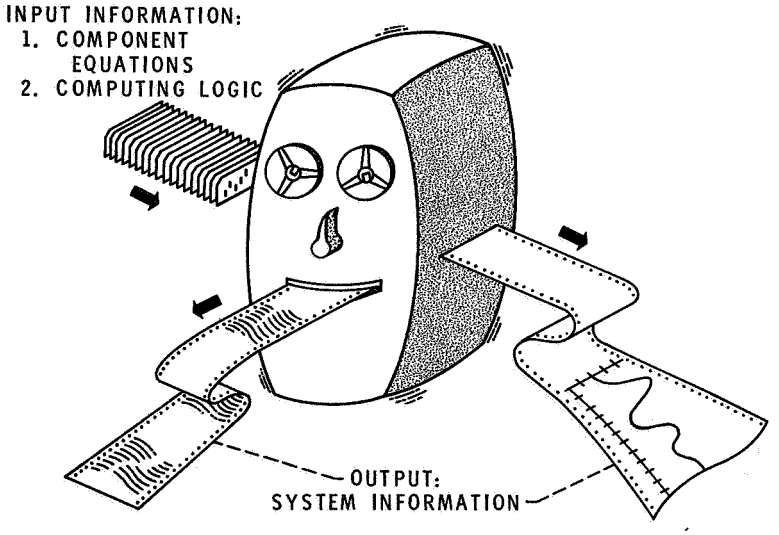

Figure 2-50. - Computer simulation.

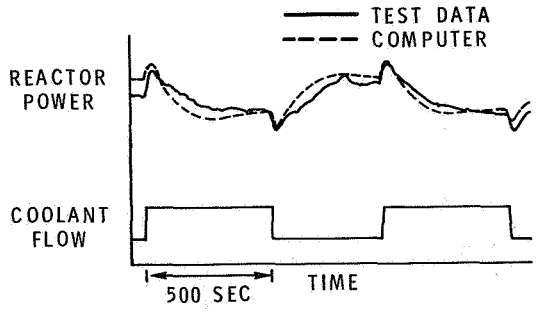

Figure 2-51. - Comparison of reactor simulation with test results.

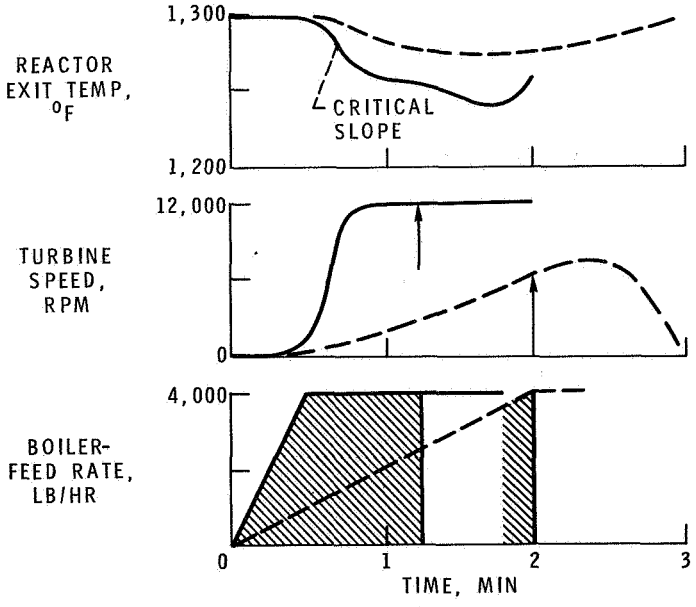

Figure 2-52. - Typical startup problem.

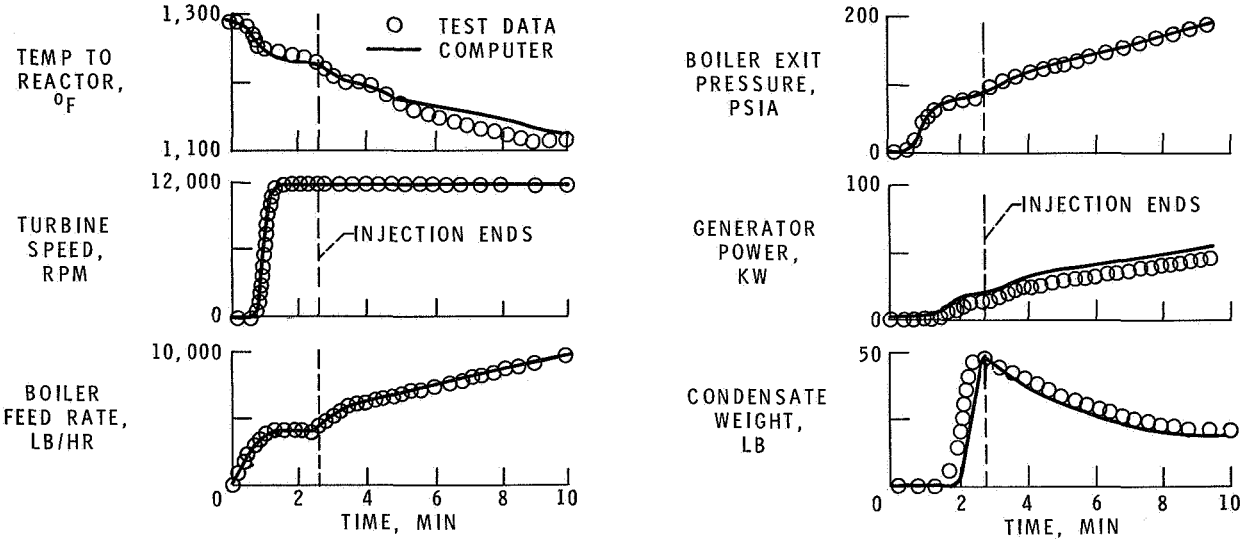

Figure 2-53. - Comparison of test and computer results.